ANALYSIS OF EVAPOTRANSPIRATION WATER FLUXES AT A FLOODPLAIN TUNDRA IN THE LENA RIVER DELTA

Master Thesis

M.Sc. Program for Polar and Marine Science POMOR

Saint Petersburg State University / Hamburg University

by

Vitalii Samoilenko

Saint Petersburg / Hamburg, 2017

ANALYSIS OF EVAPOTRANSPIRATION WATER FLUXES AT A FLOODPLAIN TUNDRA IN THE LENA RIVER DELTA

Vitalii Samoilenko
Master Program for Polar and Marine Sciences POMOR / 02200 Ecology and environmental management
Supervisors:
Prof. Dr. Lars Kutzbach, Hamburg University, Institute of Soil Science, Germany
Prof. Dr. Kirill Chistyakov, Saint Petersburg State University, Institute of Earth Science, Russia

Evapotranspiration (ET) plays an important role not only in coupling the water and energy supplies but also at controlling emissions of carbon from the soils in form of CO_2 or CH_4 in Arctic landscapes underlain by permafrost. Despite the fact that floodplains territories appear to be a huge carbon pool, in comparison with the ice-wedge polygonal tundra, little attention so far has been paid to them. Due to this gap, the current study is focused on the estimation and modeling of ET fluxes at heterogeneous tundra conditions of an active floodplain of Samoylov Island situated in the Lena River Delta by applying the eddy covariance technique. During the measurement campaign in 2014 and 2015, the estimated mean ET fluxes amounted to 0.057 mm h^{-1} and 0.048 mm h^{-1} respectively. These differences are coupled with lower amount of net radiation and predominance of cloudy conditions over the second observation campaign. Furthermore, a large variability in the range of ET fluxes over the seasons is linked with the unevenly distribution of ET sources at the constantly changed footprint area. In general, Priestly-Taylor (PT) approach allows getting stronger correlation between the modeled and observed values of ET than Penman-Monteith (PM) method during the measurement campaigns. Nonetheless, PT approach allows estimating better results for the first half of measurement campaigns, while the PM – for the second. Explaining this variability is based on the better performance of approaches depending on the hydrometeorological and environmental conditions. Furthermore, the deterministic model of footprint area has been enabled to estimate the ET fluxes from three vegetation classes. In turn, formed obtained values from each vegetation class have been used to estimate ET rates during the seasons for the entire floodplain territory. Thus, during the 2014 measurement campaign was observed the prevalence of ET on the precipitation, while the 2015 – the opposite. Overall, employing of obtained ET fluxes on the ecosystem scale is crucial not only for the accurately estimating of the hydrological cycle but also for modeling greenhouse gases emissions.

Анализ потоков эвапотранспирации на примере пойменного участка в дельте реки Лены

Самойленко Виталий

Магистерская программа «Полярные и морские исследования» («ПОМОР») / 022000 «Экология и природопользование» Выпускная квалификационная работа магистра
Научные руководители:
Профессор, д.г.н. Куцбах Л., Гамбургский университет, Институт Наук о почве, Германия
Профессор, д.г.н. Чистяков К.В., Санкт-Петербургский государственный университет, Институт Наук о Земле, Россия

Процесс эвапотранспирации (ЭТ) играет важную роль не только в один из важнейших элементов гидрологического и энергетического балансов, но также оказывает значительное влияние на форму эмиссии углерода из почв (в виде CO_2 или CH_4) в арктических ландшафтах, подстилаемых многолетней мерзлотой. Несмотря на то, что в верхних слоях почвы пойменных территорий хранится большое количество углерода, по сравнению с территориями полигональной тундры им уделяется мало внимания. В связи с этим, данное исследование было сфокусировано на оценке и моделировании потоков ЭТ в гетерогенных условиях тундры на примере поймы Самойловского острова, расположенного в дельте реки Лены, с применением техники вихревой ковариации. Во время измерительной кампании в 2014 и 2015 гг. средние расчетные потоки ЭТ составляли 0,057 мм $ч^{-1}$ и 0,048 мм $ч^{-1}$ соответственно. Эти различия объясняются тем, что в период второй измерительной кампании преобладала пасмурная погода и, как следствие, количество поступающей коротковолновой и длинноволновой радиации к поверхности земли было существенно меньше. Кроме того, большая изменчивость потоков ЭТ в течение сезонов связана с учетом неравномерного распределения источников ЭТ вокруг измерительной башни. В целом подход Пристли-Тейлора (ПТ) позволяет получить более сильную корреляцию между смоделированными и наблюдаемыми значениями ЭТ, чем метод Пенмана-Монтейта (ПМ) для обеих измерительных кампаний. Тем не менее, подход ПТ позволяет получить лучшие смоделированные значения для первой половины измерительных кампаний, тогда как ПМ - для второй. Это связано с учетом в методологиях расчётов этих методик специфических особенностей гидрометеорологических и экологических условий, преобладающих в начале или конце сезона. Кроме того, детерминированная модель зоны источников вихрей

позволила подразделить рассчитанные ЭТ потоки на три различных классов растительности. В свою очередь сформированные полученные значения для каждого класса растительности были использованы для оценки ЭТ потоков для всей территории поймы. Таким образом, в течение 2014 года было отмечено преобладание ЭТ потоков над количеством выпавших осадков, когда как в 2015 году наоборот. В целом использование полученных значений потоков ЭТ в мезомасштабе имеет чрезвычайное значение не только для точной оценки гидрологического цикла, но и для моделирования выбросов парниковых газов.

Contents

1. Introduction and aims

The Arctic is one of the world regions susceptible to the greatest climate changes (Polyakov et al., 2003). Over the last 100 years, the average temperature in the Arctic has raised at nearly twice the rate of the global average (IPCC, 2007). Many models predict a further temperature increase over the Arctic territories from 3 up to 10°K (Giorgetta et. al, 2013). As a result, prognosticated warming of the northern high latitudes will have significant effects not only in the Arctic region, but also make an impact on the global climate system via changes in the processes of energy exchange, moisture and greenhouse gases (Wood et.al, 2009, Oberbauer et al., 1996).

According to research it is estimated that up to 18% of northern hemisphere land surface is underlain by permafrost (Zhang et al. 2000). Permafrost is soil, sediment or rock with temperatures continuously below 0 °C for more than 2 years (van Everdingen, 1998). Due to harsh environment conditions, characterized by cold temperatures and oversaturated soil water conditions, the process of organic matter decomposition in permafrost regions is constrained (Ping et. al., 1998). As a consequence, permafrost-affected soils are a huge store of carbon and nutrients with the stocks of 1300 ± 200 Gt C (Hugelius et al., 2014). However, according to the future warming scenarios, the increase of the permafrost thawing level may lead to the transformation of the permafrost-affected soils from a sink of carbon to a source of carbon (Zimov et al., 1997). Previously frozen organic carbon stored in these soils will be released to the atmosphere in the form of one of the greenhouse gases CO_2 or CH_4, initiating further warming and creating a positive feedback cycle (Beer, 2008).

In high-latitude conditions, many scientists have observed a tight interrelation between the energy, biogeochemical and hydrological cycles (Figure 1) (Strack et al., 2004, Kutzbach, 2006). The hydrological cycle in the Arctic conditions has a great amount of compounds but in comparison with others, the role of evapotranspiration process is very difficult to neglect. The term evapotranspiration (ET) combines two fluxes associated with different ways of water vaporization in environmental systems: (1) abiotic water evaporation (from open water sources, soil pores, surfaces of leaves), and (2) biotic leaf transpiration (diffusion of water from the leaf to the atmosphere via the stomata) (Katul et.al, 2011). ET, or latent heat flux, plays a key role in coupling the water and energy supplies in Arctic landscapes underlain by permafrost such as the Lena Delta (Muster et al., 2012). Consequently, during summer time the latent heat flux is the main mechanism of surface energy dissipation (Kane et al., 1990). According to Kutzbach [2006], more than 40% of gained net radiation during the summer is

consumed by the latent heat flux in conditions of polygonal tundra. Due to the expected future warming and consequent changes of the energy balance at high latitudes, significant changes in the hydrological cycle can be expected mainly via the process of ET. The hydrological cycle plays the key role for the gas exchange with the atmosphere in northern wetlands through determining oxic or anoxic soil conditions and respectively which gas (CO_2 under oxic conditions, CH_4 and CO_2 under anoxic conditions) will be released (Friborg et al., 2003, Strack et al., 2004). Because of this, to understand future possible changes in the carbon cycle, it`s necessary to take into account not only direct impact of thawing of permafrost, but also changes in the Arctic hydrological cycle.

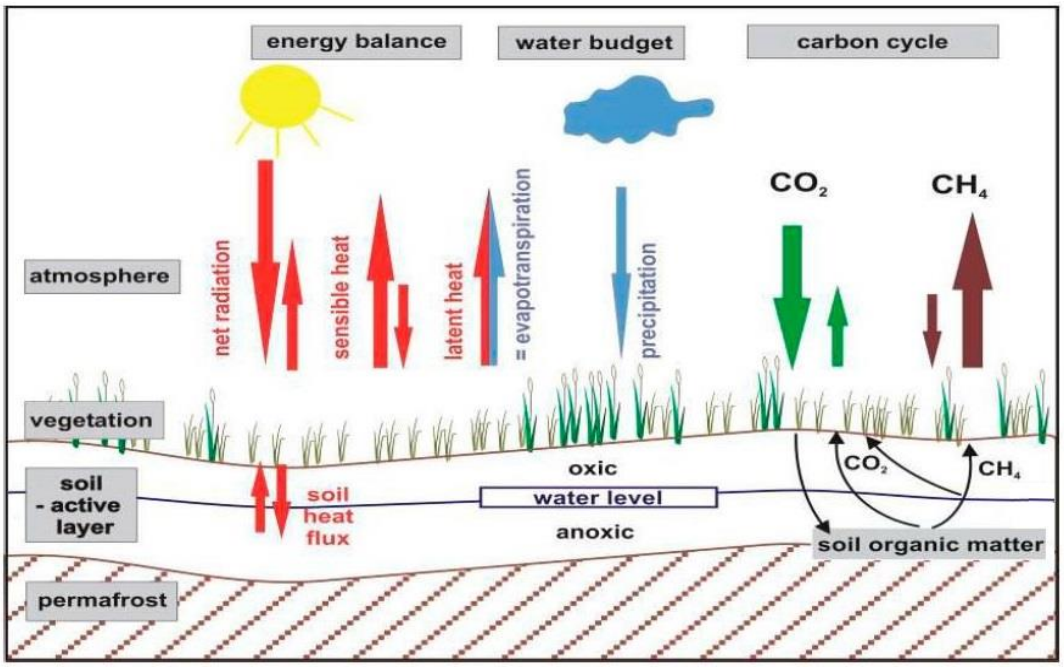

Figure 1. Land-atmosphere interactions between energy balance, water balance and carbon cycle in permafrost environments. (Source: Kutzbach, 2006).

Despite the importance of ET as a water flux associated with energy transformation, the problem of how it will be affected by possible climate changes is unclear (Woo et al., 2008). On the one hand, some scientists tend to believe that ET fluxes will be increased (Vihma et al., 2015), but on the other hand, some of them suppose that rates of ET will be unchanged (Rouse et al., 1992). According to the opinion of Woo [2008], such diverse views on the possible effects exist mainly because of the absence of long-term hydrological and climatological data-sets and the influence of high spatial heterogeneity in Arctic wetlands with regard to hydrological processes.

Currently a great variety of studies are focused on the investigation of the hydrological cycle under permafrost conditions mainly at the macro or micro scales

(Woo et al., 2008). Thus, satellite techniques are common for global researches, while for the small-scale studies such methods as using a dynamic lysimeter or portable chamber become popular (Muster et al., 2012, Cohen et al., 2015). However, due to some errors of data obtained by the satellite remote sensors, and difficulties in accounting processes occurring at the micro-scale level, the meso-scale effect of spatial heterogeneity of ET is not taken into account during measurements mentioned above. Nevertheless, the effect of high spatial environment heterogeneity is strong represented in the Lena River delta and other areas of Siberia and Alaska (Woo et al., 2008). According to Muster [2012], leaving aside the issue of spatial heterogeneity can adversely affect the assessment of ET fluxes at global and regional models. In spite of this, eddy covariance (EC) method can be attributed to the intermediate niche of measurements between the mentioned above macro- and microscale techniques of observation. Thus, this method allows estimating the rates of energy, water and gas exchange between the land and atmosphere, on the ecosystem level (Landerer et al., 2010, Burba and Anderson, 2007). Nowadays EC technique of observation has become a popular and accurate tool to study the turbulent exchange fluxes of energy and matter in the environmental conditions of high latitudes (Wille et al., 2008, Kutzbach, 2006, Landerer et al., 2010)

Despite the great amount of studies, which are focused on the possible changes in the hydrological cycle and energy balance at the extremely high-latitude climate conditions, little attention so far has been paid to the floodplain areas, which are widespread within the valleys of the large Siberian rivers. Nevertheless, they appear to be a huge carbon pool with a mean soil carbon stock in the upper 1 m of 14 ± 7 kg m^{-2} in the Lena River Delta and could represent almost a half of soil-covered territories of arctic river deltas (at the example of Lena River delta) (Zubrzycki et al., 2013).

Due to this gap, this study focusses on one important element of the hydrological cycle and energy balance at the earth`s surface - ET fluxes at a heterogeneous tundra landscape with variable mesorelief and vegetation cover by the example of an active floodplain on Samoylov Island in the Lena River Delta. According to that, the aims of the study are:

i) to compare the accuracy of different approaches for ET estimation at floodplain environmental conditions;

ii) to test different methods of ground heat flux estimations and their influence on the modeled results;

iii) to analyze spatial and temporal variability of the calculated and modeled ET fluxes;

iv) to define the role of different vegetation types for the landscape ET flux budget.

2. Fundamental concepts of permafrost hydrology

2.1. Features of hydrological cycle at permafrost environmental conditions

The hydrological cycle at permafrost environmental condition is characterized by a number of similarities and differences compared to non-permafrost areas (Woo, 2012). Thus, for example, the amount of unfrozen water in frozen soil decreases considerably when the temperature falls below freezing limit (Woo, 2012). Nevertheless, due to the dissimilarities, the permafrost hydrology differs in more aspects compared to the hydrology of landscapes which are non-underlain by permafrost.

Firstly, due to prolonged freezing conditions in the permafrost areas, the main variable for development of hydrology in the permafrost environment is the depth of thawing front during the summer season – the thickness of the active layer (Carey and Woo, 1998). The depth of seasonal thawing and distribution of the frost table regulate on-surface and near-surface hydrological processes such as water storage capability, water infiltration, and routing of water flows (Woo, 1986, Kane and Chacho, 1990). During the soil thawing period over the summer season, the thickness of the active layer increases, which leads to an expansion of the water-saturated zone within the soil profile. Nevertheless, changes in the active layer thickness are controlled by many factors such as type of permafrost integrity, physical and thermal properties of the surface cover and soil, ice-content in the soil, vegetation type, soil moisture and others (Brown et al., 2000; Zhang et al., 2005). Thereby, in case of high-latitude regions, where frozen ground is often oversaturated with ice, the active layer plays a role of storage for the most of the surface water flows (Woo, 2012). Moreover, this often shallow and water-saturated unfrozen horizon directly affects runoff and water flows, which are linked with the snowmelt and summer precipitation (Yamazaki et al., 2006; Koch et al., 2014), as well as nutrient transport (Koch et al., 2013).

Secondly, the presence of a permafrost layer influences not only on the surface water flows, which could not provide groundwater reserve recharge, but also the groundwater. Groundwater from below the permafrost rarely reaches the surface and

there is much less interfusion between near-surface and deep-seated groundwater in permafrost than in non-permafrost areas (Woo, 2012).

Thirdly, the existence of water in three aggregate states not only above the surface, but also below it, leads to the development of an even closer relationship between energy and water fluxes (Woo, 2012). Thus, mainly the processes of permafrost thawing and evapotranspiration need energy in the form of latent heat which couples the energy and water fluxes (Muster et al., 2012).

Fourthly, in high latitudes the frost action processes and related to them periglacial geomorphology features have a great effect on the surface and subsurface water movement (Woo, 2012). As a result of frost action processes and uneven thawing of the permafrost sub- and subsurface water flows prefer pathways, which are linked with networks of cracks, pipes or tunnels, depressions on buried bedrock surfaces or frost table configuration (Trochim et al, 2016, Pidwirny, 2006).

Finally, permafrost has another mechanism to affect water and energy fluxes – via vegetation. Due to the fact that the growth of plants' root system down in the permafrost environment is prevented, water uptake and consequently transpiration ability is limited compared to areas not underlain by permafrost (Billings and Mooney 1968, Woo, 2012).

Moreover it`s necessary to underlain the important hydrological peculiarity of the floodplain territories at permafrost environment conditions – close relationships with the large watercourse. On the one hand, proximity of lowest parts of the river terrace to the streams leads to floodplain areas flooded during the spring flood periods. After the flooding, superfluous water recharge stored water masses resources on these territories and contribute to the development of temporary watercourses and the redistribution of incoming water resources. Thereby, the hydrological cycle of the floodplain territories is closely linked not only with the snow and permafrost thawing resources but with the superfluous water incoming over the flooding period (Donchenko, 1987). On the other hand, proximity of floodplain areas to the stream leads to the redirection of surface and subsurface water movement mainly to the riverbed and rapid discharge of water reserves.

Moreover, the presence of continuous permafrost also influences the water balance. Thus, due to limited connection between surface and groundwater resources, during the summer season the water balance can be described as a simple equation:

$$\Delta S = P - Q_g - Q_s - ET \qquad (1)$$

where ΔS is storage change over time, which includes changes in storage water resources in the soil, aquifer, snow banks and in other forms, P – is precipitation input, Q_g – lateral discharge of groundwater flows through the active layer, Q_s –surface runoff and ET – evapotranspiration flux (Rovanesk et al., 1996, Hong and Gourley, 2014)

Rovanesk found that in high latitudes due to prevalence of a low gradient in landscapes, the role of surface and groundwater discharge is diminished on the example of arctic wetlands (Rovanesk et al., 1996). Based on this fact, the vertical hydrological fluxes such us P and ET predominantly control water balance in Arctic environment (Woo et al., 1992). Moreover, Rovanesk noticed that the ET flux exceeds summer precipitation in summer and it is a major mechanism of summer water loss for these areas (Rovanesk et al., 1996). Despite the proximity of floodplain areas to the riverbed and as a consequence increase of impact of surface and groundwater runoff at the water balance equation, presumably the role of ET remains significant.

Based on the important role of ET fluxes in the water balance mentioned above, much attention was paid to estimate the main factors that affect this process. Thus, the rate of ET is controlled by hydrometeorological and environmental groups of factors (Wang & Dickinson, 2012; Williams et al., 2012).

The first group includes such parameters as availability of free energy and water, which is linked with the amount of net radiation and precipitation, respectively (Rouse, 2000, Almusaed, 2010). Moreover, this group includes two other important factors - vapour pressure deficit (VPD) and wind speed above the surface (Burba and Anderson, 2007, Wu et al., 2010). Thus, the evapotranspiration rate is higher if it occurs in dry air. Additionally, if wind removes saturated air by another portion of dry air, the potential of evapotranspiration will be increased (Saha, 2012).

The second group consists of factors linked with the characteristics of vegetation and soil. Thus, such plants parameters as type of root, leaf area index, reflectivity of plant surfaces and many others affect the evapotranspiration rate (Almusaed, 2010). Besides, the stomata resistance is a key factor, which controls biotic transpiration. The status of stomatas controls the amount of water that transpires through the leaves of plants (Saha, 2012). Such soil characteristics as albedo, texture and heat capacity, which influence the evapotranspiration process, also must be taken

into account (Saha, 2012). Based on this, spatial heterogeneity at arctic tundra and linked with it the factors mentioned above, creates difficulties at the modelling and predictions of ET fluxes. The impact of such factors as water table position on the ET rates is still being studied (Sonnentag et al., 2010).

2.2.Impacts of climate change on the permafrost hydrological cycle

There is a lot of evidence of air temperature rising in in the Arctic region (Osterkamp, 2005; Romanovsky et al., 2010). Many scientists agree on their forecasts that this positive trend will continue in the future, which will affect the large-scale degradation of permafrost (Pastick et al., 2015). One of the obvious consequences of air temperature rising in high latitudes is an increase of active layer thickness (ALT). Nevertheless, scientists have noted a large inter annual variability and the lack of a constant increase in the dynamics of ALT (Osterkamp, 2005, Harris et al., 2009). Probably, this is largely due to the fact that hydrological elements such as soil moisture and thickness of the snow cover have a significant influence on soil characteristics (for example, on their heat capacity or heat conductivity) and as a consequence affect the development of thickness of the active layer during summer periods (Jorgenson et al., 2010).

Climate change in the Arctic can lead to significant changes in surface and subsurface hydrology in the Arctic region. Thus, changes in the distribution of permafrost can affect surface and subsurface routing of water flows, storage capacity and drainage flow at in-situ, local and regional scales by different ways (Figure 2).

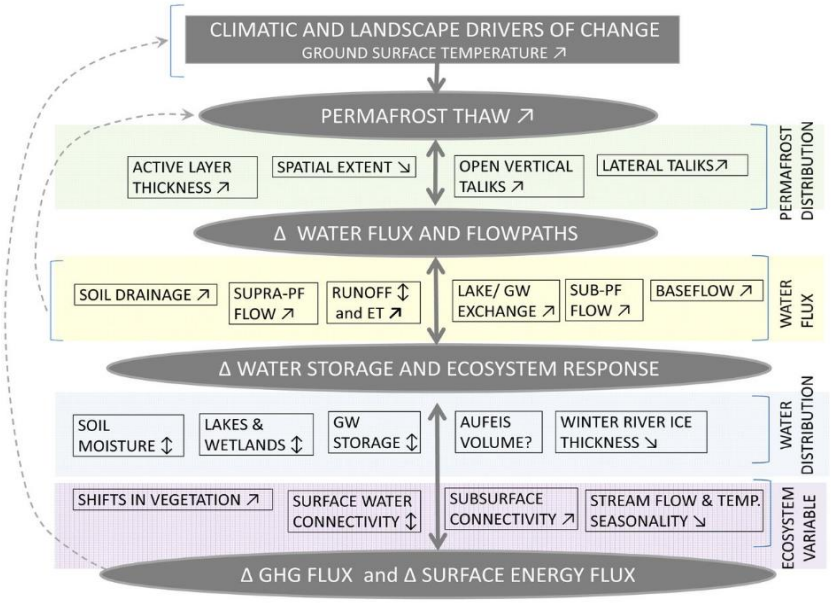

Figure 2. Overview of the effects of permafrost thaw on water fluxes and distribution (Source: Walvoord et al., 2016)

Firstly, due to an increase at the depth of seasonal thawing, previously blocked vertical and lateral pathways for water flows will be available to develop. Thawing of permafrost can enhance surface and subsurface water fluxes, drainage, connection and exchange of groundwater reserves. Based on this, the arctic hydrological system will transform from the surface water-dominated type to a groundwater-dominated system (Walvoord et al., 2016). Also, thawing of permafrost can lead to significant changes in arctic landscapes (Quinton et al., 2011). So the development of such processes as thermokarst or ground subsidence can affect the storage, routing and runoff of surface and subsurface water flows (Connon et al., 2014).

Secondly, in addition to the potential large-scale redistribution of surface and near-surface water in the summer months, changes in water stored as ice in the winter period are expected (Walvoord et al., 2016). As a result of groundwater runoff increase during freezing time, more ice will be formed along the watercourses and create masses of layered ice (Woo, 2012). It is expected that ice breaks, which usually occur in spring, can be activated in the middle of winter due to warm periods. Thus, the observed warm periods in the middle of the winter season have already caused significant ice jams and floods at the rivers of the middle of Canada (Beltaos, 2002), and such events may become more prevalent in the near future in the Arctic region.

Thirdly, the air temperature rising in high latitudes as well as changes in the distribution and storage of surface and subsurface water resources, will directly affect arctic ecosystems (Henry & Molau, 1997, McGuire et al., 2002). In the future and in some areas of high latitudes already observed, changes in vegetation include shifts in species range, phenology and vegetation composition (Arft et al., 1999, Jorgenson et al., 2001, Myers-Smith et al., 2011). Thus, all changes in ecosystems mentioned above will create feedback interactions, which will effect hydrological and energy balance at different scales (Myers-Smith et al., 2011). For example, shrub expansion in the high Arctic will lead to increased rates of ET during summer due to an increase in leaf area cover and will significantly impact summer and winter energy balance by lowering surface albedo (Eugster et al., 2000, Juszak et al, 2014).

The expected increase in productivity of arctic ecosystems will affect carbon cycle dynamics (Schuur et al., 2007). At the same time, carbon release as a result of the intensification of heterotrophic respiration and intensity of decomposition of organic matter may exceed the projected growth of primary productivity as a result of warming (IPCC, 2001). Moreover, the predicted changes of hydrological conditions also play an important role on the dynamics of the carbon cycle and emissions of greenhouse gasses

(Petersen et al., 1984). One of the most important factors controlling the process of carbon burial in soils is the amount of soil moisture and, as a consequence, prevalence of anaerobic or aerobic conditions in the soil (Billings et al., 1982). For most territories of the Arctic (especially for wetlands) in case of preservation of the rising temperature trend and maintaining the current moisture regime in soils, an increase in CH_4 emissions is projected (Hassan at el., 2005). In this case, the release of CH_4 only from the territory of the Arctic wetlands can be equal to anthropogenic emissions (Gedney at al., 2004). If the temperature rise in high latitudes is accompanied with the decrease in the level of groundwater, Arctic territories could transform from storage to a source of CO_2 (Davidson and Janssens, 2006).

Moreover, activation of soil drying processes is possible not only in case of a decrease in groundwater level. Increasing the duration of the vegetation period, leaf-cover area, changing the types of the root system can lead to an increase of evapotranspiration rates during the summer. Thus, in the Alaskan Arctic, an increase in ET has already observed, which led to greater dominance of the evapotranspiration flux over precipitation in the summer and, consequently, drying of the soil (Oechel et al., 2000). However, due to the complex interaction between the effects of warming, permafrost thawing, hydrological and energy cycles in the Arctic, future changes can not be predicted with high reliability.

3. Material and methods

3.1.Study site description

The investigation site was located in the zone of continuous permafrost, on one of the islands in the Lena River Delta (Brown and Haggerty, 1998) (Figure 3). The Lena River Delta is located on the northern coast of Siberia, at the interface between Eurasia and the Laptev Sea, a part of the Arctic Ocean. The average annual Lena River discharge is close to 5.29 x 103 m^3, and about one-third of water runoff is observed during the period of summer flooding in the June (Ivanov and Piskun, 1998, Fedorova et. al, 2015) According to Fedorova [2015], since the 1980s water discharge has increased that could be linked with the air temperature rising in the Arctic region and active permafrost thawing in the Lena`s catchment area. The land area of the delta occupies 32 000 km^2, which makes the Lena River Delta one of the largest in the world and the largest in the Arctic (Walker, 1998). The fan-shaped delta is consists of more than 1500 islands and can be subdivided to three different geomorphological river terraces units (Grigoriev, 1993).

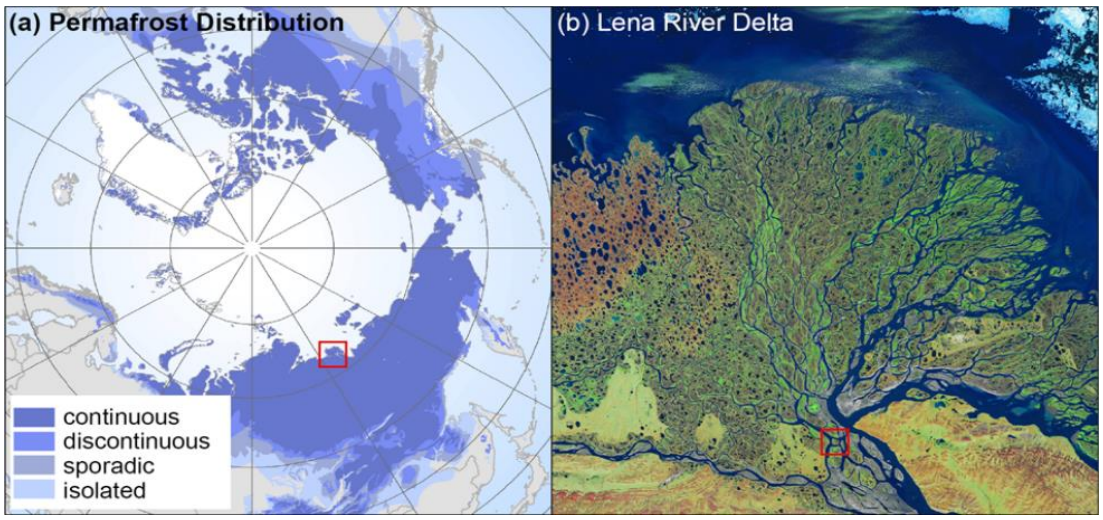

Figure 3. A- Types of permafrost in the Northern hemisphere (Brown et al., 1998) and location of the Lena River Delta; B - Location of the Samoylov island within the Lena River Delta (source: Boike et al., 2013)

Samoylov Island is a good representation of modern geomorphological processes that occur in the Lena River Delta. It has an area of 5 km^2 and is subdivided in two geomorphological units: the eastern part (~ 3 km^2) – the Late-Holocene river terrace and the western (~ 2 km^2) - the active floodplain, which is annually flooded by the Lena River (Kutzbach, 2006) (Figure 4). The floodplain area of the Samoylov Island strongly depends on the water level. During the flood peak, usually observed at the beginning of June, which is linked with the snowmelt and commonly accompanied with ice dams, the floodplain area is mostly covered with water. Nevertheless, the area prone to flooding varies from year to year. On the other hand, during the autumn the floodplain area could reach size of 2 km^2, when the water level of the Lena River is lowest. The investigation site was located on the western part of Samoylov Island.

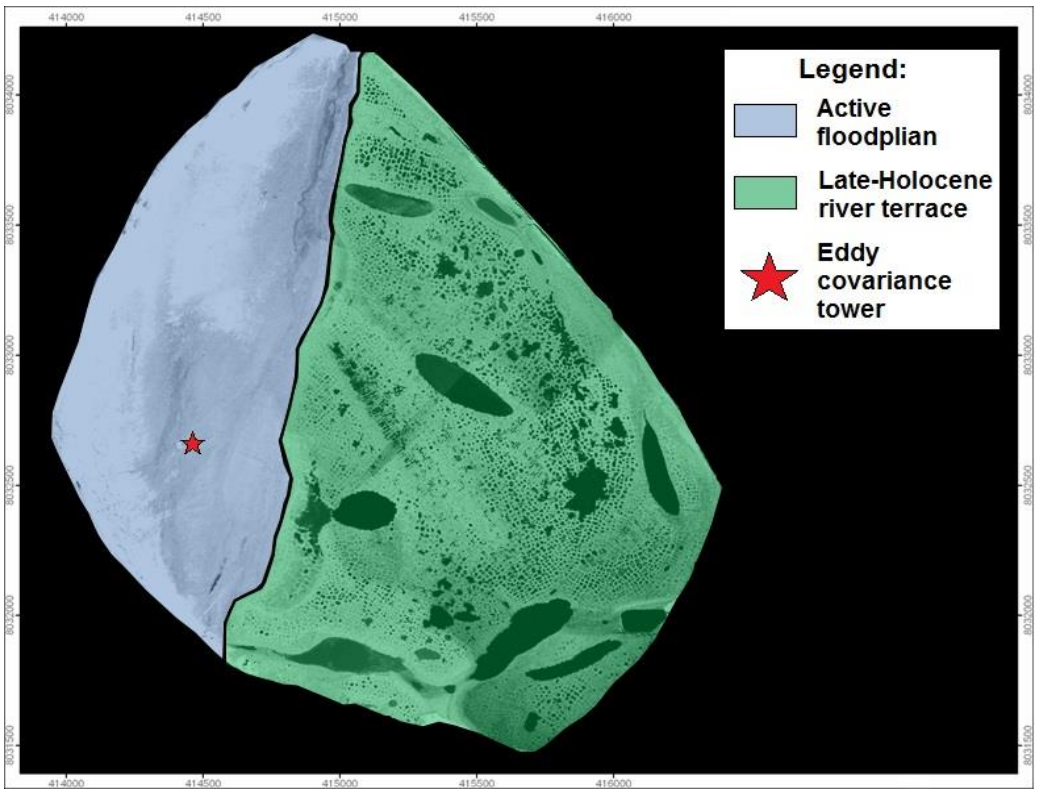

Figure 4. Geomorphological units of the Samoylov Island. Position of star shows the location of the eddy covariance tower (modified after Boike et. al, 2012)

3.2.Climate

The climate in the Lena River delta is continental-arctic, characterized by low air temperatures and precipitation. The mean annual air temperature on Samoylov Island was -12.5°C during the period between 1998-2011 (Boike et. al, 2013). Thus, the mean air temperatures of the coldest month February and the warmest month July are –33.1°C and +10.1°C respectively (Boike et. al, 2013). The mean value of summer precipitation on Samoylov Island was 125 mm during the period between 1998-2011 (Boike et. al, 2013). Nearly three quarters of all rainfall events, which occur from the middle of May until the end of September, are observed in the light form, with less than 1 mm precipitation (Boike et. al, 2013). The amount of precipitation that fall in the form of rain during the growing season from mid-June to mid-September is approximately equal to the precipitation that falls in the form of snow and accumulates during the cold period (Kutzbach, 2006).

The Lena River Delta is located at the border between the Arctic Ocean and the Siberian continental land; because of this, the synoptic weather conditions in this area are strongly depending on the wind direction. During the spring, summer and autumn seasons, usually northern winds, which tend to be associated with the passages of North

Atlantic cyclones, transport cold and humid air masses. Southern winds, which are lined with the Siberian High, bring warm and dry air to this place (Serreze et. al, 1993).

3.3.The eddy covariance method

The eddy covariance (EC) method is one of the most prominent techniques used to determine exchange rates of energy, water and trace gases between the land and near-surface atmosphere (Burba and Anderson, 2007). The concept of the EC method is based on turbulent transport theory and systematic sampling of physical properties of turbulent air parcels to estimate exchange rates of quantities of interest between the land and atmosphere (Priestley, 1959, Foken, 2017). The main idea of the EC method is that the vertical flux could be represented as a covariance of measured vertical wind speed (upward and downward air movement) and concentration of the studied substance (Foken and Kretschmer, 1990, Baldocchi, 2005). Nevertheless, in order to realize this idea two assumptions are applied. Firstly, it is assumed that the density fluctuations are negligibly small in comparison with the oscillations of other quantities (Lee et al., 2004). Based on this assumption, most of the eddy covariance measurements are applied to obtain data from homogeneous and flat landscapes (Finnigan, 2003, Aubinet et al., 2005). Secondly, for periods of the order of half an hour, the vertical flow over a horizontal homogeneous terrain is assumed insignificant so there is no divergence or convergence of the flow (Leclerc and Thurtell 1990).

The EC method has many advantages. First of all, this method permits to do long-term and direct measurements without any impact and disturbances at the land surface (Foken and Wichura, 1996). Moreover, the EC technique allows collecting data in high temporal resolution at ecosystem scale in the upwind direction – the footprint area (Gash 1986). However, the EC method is a complex measurement method that requires careful processing and strict adherence to the above conditions in the obtained data (Burba and Anderson, 2007). Moreover, the EC technique has several flaws. For example, (1) the incomplete closure of the energy balance (especially at night when the turbulent processes are weakening) (Wilson et al., 2002, Foken, 2017); (2) the threats of advection influence on the observed processes (Aubinet et al., 2005); (3) the violation of the homogeneity assumptions due to diverse vegetation and topographical characteristics in the footprint area (Aubinet et al., 2002).

3.4.General EC setup

Measurements were taken from an EC system, which was installed in the southern part of the floodplain of Samoylov Island. Measurements were organized during two campaigns and span periods from 18th June – 15th September 2014 and 9th June to 23th September 2015.

A three-dimensional sonic anemometer (CSAT3, Campbell Scientific, Inc., UK) and an open-path infrared gas analyzer (LI-7500A, LI-COR Biosciences, Inc., USA) were installed at the flux tower to measure the vertical turbulent fluxes of water vapor. Instruments were mounted at a height of 2.83 m. All output data from these devices was recorded on a data logger (LI-7550, LI-COR Biosciences, Inc., USA) at a frequency of 20 Hz.

Ancillary measurements were obtained at the floodplain to provide meteorological data including air temperature and relative humidity (HMP45, Campbell Scientific, Inc., USA), atmospheric pressure (CS100, Campbell Scientific, Inc., USA), incoming and outgoing solar radiation (NR01, Hukseflux Thermal Sensors B.V., Delft, The Netherlands). Moreover, in order to obtain the data of dynamic changes of soil temperature during the two campaigns at the floodplain area, a network of measurement posts was organized. At each post, soil thermometer (TH3, UMS, Germany) were installed to measure soil temperature along the profile at depths of 5, 10, 20, 30, 50 and 100 cm from the surface. All additional data was recorded on a logger (CR1000, Campbell Scientific, UK).

3.5.Flux processing

The calculation flow was carried out using EddyPro software (version 6.0.0, LI-COR Biosciences, Inc., USA) for intervals of half an hour. The raw data processing procedure included the following steps: (1) the detection of randomly erased peak values (very large or very small) due to electronic noise and their replacement by running means values (Vickers & Mahrt, 1997); (2) the double rotation of the 3-D wind coordinate system in order to eliminate the contamination of the vertical wind by the horizontal wind components (McMillen, 1988); (3) averaging over half-hour intervals with the purpose of calculating turbulent fluxes; (4) cross correlation of time series data obtained by an anemometer and the gas analyzer, respectively, in order to compensate for the time delay between the wind signals and the gas analyzer signals (Foken et. al, 2004); (5) Webb-Pearman-Leuning correction to allow and compensate temperature and water vapor fluctuations that affect the fluctuations of gases (such as CO_2, H_2O and

others) during the flux calculation (Webb et al., 1980); (6) spectral corrections in the low-frequency range due to compensation for the loss of flux as a result of averaging (Moncrieff et al., 2004); (7) spectral correction in the high-frequency range (Ibrom et al., 2007, Horst and Lenschow, 2009).

After the processing of the obtained raw data, EC methods allow calculating the scalar quantitates of turbulent sensible heat (Q_H) and latent heat (Q_E) fluxes as the covariance of the scalar with the vertical wind speed by the following formulae:

$$Q_H = \overline{w' T'_{son}} \rho_{mass,air} C_p \qquad (2),$$

$$Q_E = \overline{c' H_2O\, w'} \frac{P}{RT} \lambda\, mH_2O \qquad (3),$$

where w is the mean of vertical wind speed, T_{son} is sonic temperature, $\rho_{mass,air}$ is the air density, C_p is the heat capacity of water at constant pressure, P is the air pressure, $c\,H_2O$ is the density of water vapour in air, T is the air temperature, R is the ideal gas constant, λ is the latent heat of evaporation mH_2O is the molar mass of water. The dashes represent the fluctuations about the mean, and the overbars express the mean over the interval (Kutzbach, 2006)

Already calculated values underwent rigorous quality control in order to satisfy all the necessary conditions of the eddy covariance theory, and also provide high quality data for further modeling. Additional procedures included: (1) testing for compliance with stationary conditions (Foken and Wichura, 1996) (2) testing for sufficient development of turbulent processes (Foken and Wichura, 1996); (3) control of asymmetry and kurtosis from flux-specific scalars (Tennekes and Lumley, 1972). In cases, where the skewness was either less than -2 or greater than 2, and/or kurtosis was greater than 8, these data intervals were removed from the set (Rößger et al., 2017, in preparation). As a result of the quality assessment routine, more than 40% of flux records were omitted.

3.6.Analysis of the surface heterogeneity in the floodplain area

In order to ensure proper interpretation of data processing and ET flux modeling, an analysis of floodplain surface heterogeneity was organized. The analysis was based on a manual field vegetation classification around the flux tower and additional aerial photography, which was organized in summer 2014. The results of aerial photographs with a resolution of 8.5 cm were compared to manual classification of vegetation with subsequent adaptation, estimation of discrepancies and coincidences and obtaining final map of vegetation classes on Samoylov Island (Rößger et al., 2017, in preparation).

The relief around the investigation site is characterized as lightly wavy. Nevertheless, these slight differences in altitude have played a significant role on the surface's vegetation heterogeneity distribution. Because vegetation types and ET fluxes are strongly coupled, the distribution of these should be linked to the three indicative vegetation classes (Figure 5).

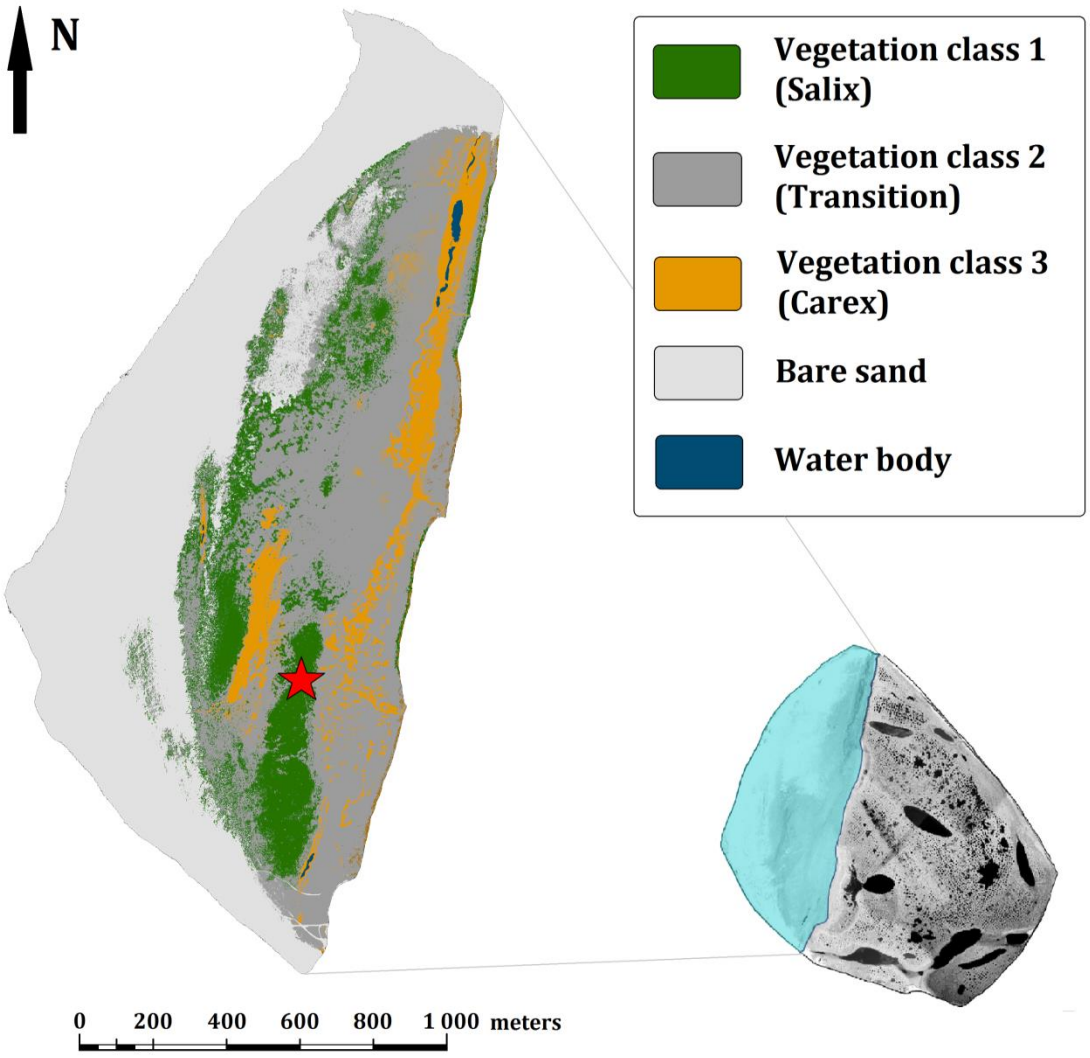

Figure 5. Vegetative classification of the floodplain part of Samoylov Island. Position of star shows a location of eddy covariance tower.

Vegetation class 1 describes areas with mostly dry top soils with good growing conditions for **shrubs** (mainly the Salix family: *Salix glauca, Salix lanata, Salix hastata, Salix pulchra*). The absence of a large amount of moisture in the soil and the shading from the shrubs only allowed the development of thin formations of moss. This vegetation is typical for an elevated sandy ridge, which dissects the floodplain in north-south direction. This vegetation class occupies 24% of the total floodplain area (251 890 m^2).

Vegetation class 3 refers to wet areas with standing waters where **sedges** (such as *Carex chordorrhiza*, *Carex aquatilis*, *Carex concolor*), *Equisetum* and *Eriophorum* dominate. Moreover, such places with the abundant amount of water are attractive for mosses, which form thick patches all over this area. Such vegetation could be found at the floodplain at the lowest lands, which are located at the north-western and eastern direction from the flux tower. This vegetation class covers approximately 18% of the floodplain territory (183 910 m^2).

Vegetation class 2 is characterized as **transitional areas** between elevated, well-drained areas and depressions with water-saturated conditions. At these sites, a mixture of representative species from the 1^{st} and 3^{rd} classes could be observed: sedges and shrubs with a different thickness of mosses at the surface. This area covers about 58% of the total floodplain area (611 154 m^2).

Moreover, small water bodies are observed on the floodplain. The largest water objects are located on the western part of the floodplain territory, at the border between the floodplain and elevated part of Samoylov Island. These water bodies are largely associated with subsurface and surface runoff from the eastern part of the island during the summer. Water vapor and other gases, which were collected by air turbulences, were not observed by measurement equipment because water objects are located far away from the location of EC tower and thus do not significantly contribute to the EC flux. Furthermore, these water bodies occupy an insignificant share from the entire territory of the floodplain. Due to that, the analysis and modeling of ET at the floodplain area were based only under consideration of the three vegetation classes described above and their ET fluxes.

3.7.Footprint analysis of the EC system

The flux footprint describes the function that estimated the contribution to the measured EC flux by unit areas in the upwind area (Bai et. al, 2014, Schuepp et. al., 1990) Thus, by determining the footprint area, for each half-hour measurement period, the contribution of each region to the absorption or liberation of matter and energy can be established (Burba, 2001). In this study, the analytical model for non-neutral stratification of Kormann and Meixner was used to calculate the footprint area (Figure 6) (Kormann and Meixner, 2001). This model is based on the solution of the two-dimensional advection – diffusion equation for power law profiles of the mean wind velocity and the eddy diffusivity (Kormann and Meixner, 2001, Leclerc and Foken, 2014).

It is necessary to underline that shape and size of footprint area are not constant and change over time. According to the micrometeorological rule of thumb, in order to satisfy the EC requirements for surface homogeneity during the observation, the measurement height should be about 100 times smaller than the distance of the upwind uniform area (Bussinger, 1988, McMiller, 1988). Measurement instruments were installed at a height of 2.83 meter; thus, fluxes that were generated within a distance of about 300 meters from the EC tower were recorded and are studied in this paper. As a result of footprint calculations, for each half-hour period fractions of the three vegetation classes of the total footprint contribution (Ω_i) could be estimated. Moreover, such meteorological factors as atmospheric stability, speed of wind and crosswind and roughness length could affect the footprint shape and size influence.

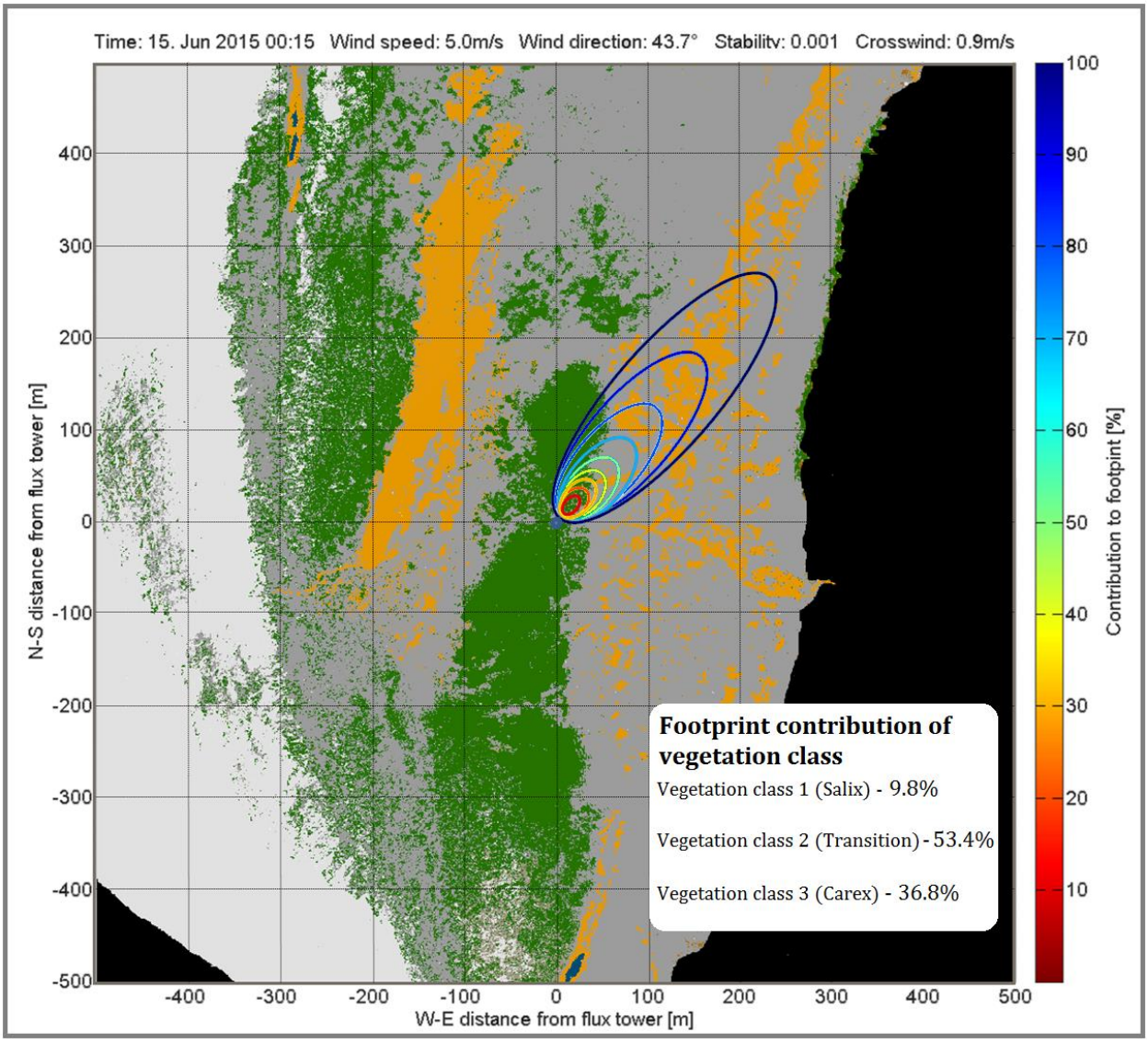

Figure 6. Footprint calculation and estimation of fractions of vegetation classes 1, 2, 3 at the footprint area (on example of measurement of 15th of June 2015 00:00 – 00:30)

3.8.Methods for modelling evapotranspiration fluxes

Temporal and spatial variability of land-atmosphere fluxes of water at the Artic environment strongly depends on the vegetation, physiographic and climatic conditions (Engstrom, 2002). At the same time, due to the limited number of the meteorological stations, transport difficulties and many other factors, the problem of temporal and spatial variations of the ET at the Arctic conditions have not been understood well yet (Kane et al., 1990, Woo et al., 2008). However, in a lack of ET data many researchers apply different models to estimate ET flux.

3.8.1. Evaporation modeling by the Penman-Monteith approach

Over the past 70 years, scientists and specialists have developed a variety of methods for calculating evapotranspiration fluxes (Blaney-Criddle, 1950; Makkink, 1957; Penman, 1948, Liebethal and Foken, 2008). The dependence of the evapotranspiration was subjected to local calibration. Limitation factors were determined for the application of techniques for wide application (FAO, 1977). Based on the analytical and experimental analysis of different methods, a group of specialists from the Food and Agriculture Organization of the United Nations (FAO) recommended adopting the combined Penman-Monteith method as a new standard for the calculation of the evapotranspiration fluxes (FAO, 1977). The Penman-Monteith method has proved to be a technique that allows predicting the ET value with high accuracy under different climatic conditions (FAO, 1977).

This approach is based on Penman's method of combining energy balance and mass transfer methods to calculate ET fluxes, as well as including aerodynamic and surface resistance factors in the equation (Penman, 1948):

$$\lambda ET = \frac{\Delta(R_n - Q_G) + Kt\left(\frac{VPD\ \rho\ C_P}{r_a}\right)}{\Delta + \gamma\left(1 + \frac{r_c}{r_a}\right)} \qquad (4)$$

Where λ is the latent heat of vaporization (Jm^{-3}), Δ is the slope of the saturation vapor pressure and air temperature curve ($kPa°C^{-1}$), VPD (kPa) is the vapour pressure deficit of the air, ($kg\ m^{-3}$), Kt is a conversion factor from a mass H_2O flux to a volume H_2O flux ($1\ m^3$ / 1000 kg), ρ is the mean atmospheric density ($kg\ m^{-3}$), r_c is the surface (bulk) resistance (sm^{-1}), r_a is the aerodynamic resistance (sm^{-1}), γ is the psychrometric constant ($kPa°C^{-1}$), and R_n and Q_G are the net radiation and surface soil heat flux, respectively (Wm^{-2}).

According to Thom [1975], the aerodynamic resistance was calculated as:

$$r_a = \frac{\ddot{u}}{u_*^2} + \frac{4}{u_*}, \qquad (5)$$

Where ü is the average horizontal wind velocity over 30 minute intervals (sm^{-1}) and u_* is friction velocity (sm^{-1}).

3.8.2. Evaporation modeling by the Pristley-Taylor approach

The Priestley-Taylor (PT) equation was developed as an alternative to the PM equation, which removes from the approach the aspect of dependence of observation. The PT model is based on the assumption of Slatyer and Mcllroy of the equilibrium of evaporation (Slatyer and McIlroy, 1961). Thus, the idea of PT approach accepts that for large and well-watered areas the radiation component of the evaporation must prevail over the advective. Moreover, if the air mass stays saturated during the contact with a wet surface, so the additions and losses of water vapor are in the equilibrium state, the atmospheric/mass transfer term from the Penman-Monteith equation could be removed (Monteith, 1965). In this case the PT approach transform to a function of available energy.

Equilibrium evaporation state occurs very rarely in natural environmental conditions due to advection processes or variations at the surface or/and atmospheric states (Eichinger, 1996). To compensate deviations between natural observations and equilibrium evaporation state Priestley and Taylor suggested using the empirical coefficient α (Priestley and Taylor, 1972). So, the PT approach for estimation of land-atmosphere heat flux is:

$$\lambda ET = \alpha \left(\frac{\Delta(R_n - Q_G)}{\Delta + \gamma} \right) \qquad (6)$$

Where λ is the latent heat of vaporization (Jm^{-3}), α is the PT empirical coefficient, Δ is the slope of the saturation vapor pressure and air temperature curve ($kPa°C^{-1}$), γ is the psychrometric constant ($kPa°C^{-1}$), and R_n and Q_G are the net radiation and surface soil heat flux, respectively (Wm^{-2}).

3.9.Methods for calculating ground heat fluxes

However, surface soil heat flux was not measured at the investigation site during the measurement campaign. In this study, values of Q_G were calculated for the measurement period using two approaches.

3.9.1. Estimation of ground heat fluxes from the Energy Balance equation

Based on the law of energy conversation, sum of all elements of energy balance that reach or leave the earth`s surface should equal zero:

$$Q_s^* + Q_H + Q_G + Q_E + \Delta Q_s + \Delta Q = 0 \qquad (7)$$

Where $-Q_s^*$ is the net radiation at the ground surface, Q_H is a sensible heat flux, Q_G is a ground heat flux, Q_E is a latent heat flux and ΔQ_S is a stored sensible and latent energy within the air, plants and soil (Foken, 2008). Also this equation is not full without some storage of minor energy balance components and measurement errors - ΔQ. According to Kutzbach [2006], ΔQ is dominating at the period of phase change of water and large during periods of snowmelt and freezing. We could omit this value at this study because the measurement campaign was not organized at these periods.

According to Greco and Baldocchi [1996], the amount of stored sensible and latent energy within the air, plants and soil could be calculated as:

$$Q_s = z_m \left[(\rho_{da} C_{da} + \rho_{H20} C_V) \frac{\delta T_a}{\delta t} + \lambda \frac{\delta \rho_{H20}}{\delta t}\right] \qquad (8),$$

Where z_m is the measurement instruments installation (2.83 m), ρ_{da} is density of dry air (kg m^{-3}), ρ_{H20} is density of water (kg m^{-3}), C_{da} is heat capacity of dry air (J kg^{-1} °K^{-1}), C_V is heat capacity of water vapour in air (J kg^{-1}°K^{-1}), T_a is air temperature (°K) and λ is latent heat of vaporization (Jm^{-3}).

3.9.2. Calculation of the ground heat flux based on the soil temperature data

One of the main tasks of surface energy balance measurements is the correct estimation of heat flux that goes into the soil. Due to the strict rules about depths of soil thermometers installation and of meteorological observations timing in different countries, there is no common method for calculating the ground heat flux.

Many modern studies are focused on the improvement and universalization of methods for estimation the ground heat flux (Gao, 2005, Gao et al., 2009, Foken, 2008, Rutten et al., 2010). Nevertheless, Rusin's method was used in this study (Rusin, 2014). Based on Fourier's transport equations for thermal energy (Marín, 2011), after the elimination of a number of deficiencies noted by Lightman (Zeitin, 1953), the method allows to calculate the ground heat flux and value of the unified volumetric thermal conductivity (k) during each measurement period for the entire soil profile in which soil temperature measurements are taking place (Rusin & Kukanova, 2012).

In comparison with other studies, the main particularity of Rusin`s method is that the calculation of ground heat fluxes and volumetric coefficient of thermal

conductivity, require values of the soil temperature not from hard-set, but from arbitrary depths (Rusin, 2014). On the basis of Tseitin's assumptions [1953], this method uses an interpolation polynom constructed based on soil temperature data from different depths (Rusin, 2014). Moreover, it should be noted that this technique is based on a fully formed dataset and uses the central-difference approximation of temperature on time in calculations (Rusin, 2014). According to this method, the process of calculating the ground heat flux and thermal conductivity can be subdivided into several stages.

First of all, based on the installation depth of thermometers, it`s necessary to create a matrix and transform it to the Vandermonde matrix:

$$M = \begin{bmatrix} 1 & z_1 & z_1^2 & z_1^3 & z_1^y \\ 1 & z_2 & z_2^2 & z_2^3 & z_2^y \\ 1 & z_3 & z_3^2 & z_3^3 & z_3^y \\ 1 & z_4 & z_4^2 & z_4^3 & z_4^y \\ 1 & z_x & z_x^2 & z_x^3 & z_x^y \end{bmatrix}, \quad (9)$$

Where z is a depth of thermometer installation, x is an index of the deepest layer of the installation of thermometers, y is a number of depths at which measurements were taken. Moreover, elements of Vandermonde matrix was identified as $m_{i,k}$.

Then, after determining and setting H value as the largest depth of thermometer installation, and has value of the depth thermometer installation, which is nearest to the H / 2, coefficients C(k) and D(k) could be calculated as:

$$C_k = \frac{H^2}{H-h}\sum_{i=0}^{i=4}\frac{m_{i,k}H^i}{(i+1)(i+2)}\left[1-\left(\frac{h}{H}\right)^{i+2}\right], \quad (10)$$

$$D_k = \frac{hH^2}{H-h}\sum_{i=0}^{i=4}\frac{m_{i,k}H^i}{(i+1)(i+2)}\left[1-\left(\frac{h}{H}\right)^{i+1}\right], \quad (11)$$

Finally, values of ground heat fluxes and thermal conductivity could be estimated as:

$$k = \frac{\frac{1}{2\Delta}\sum_{k=1}^{k=5} D_k \; T_k(t+\Delta) - T_k(t-\Delta)}{T(t_i,0) - T(t_i,h) - \frac{h}{(H-h)}\,T(t_i,h) - T(t_i,H)}, \quad (12)$$

$$Q_G = \frac{1}{2\Delta}\sum_{k=1}^{k=5} C_k \; T_k(t+\Delta) - T_k(t-\Delta) + \frac{k}{(H-h)}\,T(t_i,h) - T(t_i,H), \quad (13)$$

However, this methodology has no application experience in high latitude environmental conditions. For example it doesn`t take into account such processes as phase transitions of water inside the soil during the calculation couple that could have given a huge impact on the ground heat fluxes.

Nevertheless, in order to obtain more accurate results, the ground surface temperature data should be used in the calculations of ground heat fluxes (Gao, 2005). Surface temperature was estimated based on the Stefan-Boltzman law and radiometer data as:

$$T_{surf} = (\frac{L_{out}}{\varepsilon\delta})^{\frac{1}{4}} \qquad (14),$$

Where T_{surf} is the ground surface temperature (°K), L_{out} is long wave radiation emitted by earth (W m^{-2}), ε is the Earth emissivity (assumed to be 0.98), and δ is the Stefan-Boltzmann constant (approximated as 5.67×10^{-8} Wm^{-2} $°K^{-4}$).

In this study, soil temperature data was obtained from a station, located 10 meters to the north from the EC tower and characterized by similar environmental and soil conditions. Soil temperature measurements were performed at depths of 5, 10, 20, 30, 50 and 100 cm.

3.9.3. Calculation of the ground heat flux based on the net radiation

Additionally, a simple approach was used for a purpose of comparison and to verify the validity of the ground heat flux values obtained by soil profile temperatures data.

According to Liebethal and Foken [2007], the ground heat flux could be represented as:

$$Q_G = R_n * p, \qquad (17)$$

Where R_n is net radiation (Wm^{-2}) and *p* is parameterization coefficient. It should be noted that the p value differs substantially in daytime and nighttime due to the fact that a significant part of net radiation is consumed by turbulent processes during the day. Also, this approach cannot be applied to the evening and morning hours, when the net radiation flux and ground heat flux are differently directed (Liebethal and Foken, 2007). Based on different hydrometeorological conditions, the *p* value could fluctuate between 0.10 and 0.50 (Fuchs and Hadas, 1972; De Bruin and Holtslag, 1982; Clothier et al., 1986). In this study, the value of *p* was estimated as 0.1.

3.10. Evapotranspiration flux modeling and up-scaling of results

As mentioned above, two approaches were used to model the observed ET flux: Penman-Montheith and Priestley-Taylor. In both cases, the observed ET flux was considered as the sum of three separate ET fluxes from each vegetation class at the floodplain`s footprint area. Thus, using the Penman- Monteith methodology, the estimated ET flux was calculated as:

$$F_{ET} = \sum_{i=1}^{i=3} \Omega_i * \frac{1}{\lambda} \frac{\Delta(R_n - Q_G) + Kt \left(\frac{VPD\ \rho\ C_P}{r_a}\right)}{\Delta + \gamma \left(1 + \frac{r_{c_i}}{r_a}\right)}, \quad (15)$$

Where F_{ET} is the net ET flux observed at the eddy covariance tower (mmh^{-1}), Δ is the slope of the saturation vapor pressure and air temperature curve ($kPa°C^{-1}$), γ is the psychrometric constant ($kPa°C^{-1}$), R_n is net radiation (Wm^{-2}), Q_G is the surface soil heat flux, respectively (Wm^{-2}), VPD (kPa) is the vapour pressure deficit of the air, ($kg\ m^{-3}$), Kt is a conversion factor from a mass H_2O flux to a volume H_2O flux ($1\ m^3$ / 1000 kg), ρ is the mean atmospheric density ($kg\ m^{-3}$), r_a is the aerodynamic resistance (sm^{-1}), γ is the psychrometric constant ($kPa°C^{-1}$), r_{c_i} is the surface (bulk) resistance of i-class vegetation (sm^{-1}) and $\Omega_i$is the contribution of vegetation class I to the for each half-hourly flux according to the footprint modelling.

In turn, when using the PT method as a base for ET fluxes calculation, the equation looks like:

$$F_{ET} = \sum_{i=1}^{i=3} \Omega_i \ \frac{1}{\lambda}\ \alpha_i \left(\frac{\Delta(R_n - Q_G)}{\Delta + \gamma}\right), \qquad (16)$$

Where F_{ET} is the net ET flux observed at the eddy covariance tower (mmh^{-1}), Δ is the slope of the saturation vapor pressure and air temperature curve ($kPa\ °C^{-1}$), γ is the psychrometric constant ($kPa°C^{-1}$), R_n is net radiation (Wm^{-2}), Q_G is the surface soil heat flux, respectively (Wm^{-2}), α_i is the PT empirical coefficient for i-class of vegetation and $\Omega_i$is the contribution of i-class of vegetation class I to the at the footprint area for each half-hourly flux according to the footprint modeling.

3.11. Subdivision for periods and features of modeling

Temporal and spatial variability of the model parameters α- and r_s at the Arctic environment was underlined in many studies (Rovanesk et al. 1996, Stewart and Rouse 1976, Kane et al., 1990). According to them, at the process of their estimation it is necessary to take into consideration seasonal changes and variability due to changes in surface wetness and the corresponding transpiration properties of the vegetation

(Mendez et al., 1998). Due to that measurement campaigns were subdivided at small periods according to changes of the T_{air} and precipitation values during the observation periods (Figure 7). These parameters were chosen because they largely determine changes in soil moisture and vegetation characteristics, which need to be considered at the assessment of α-as and r_s -as over time and space.

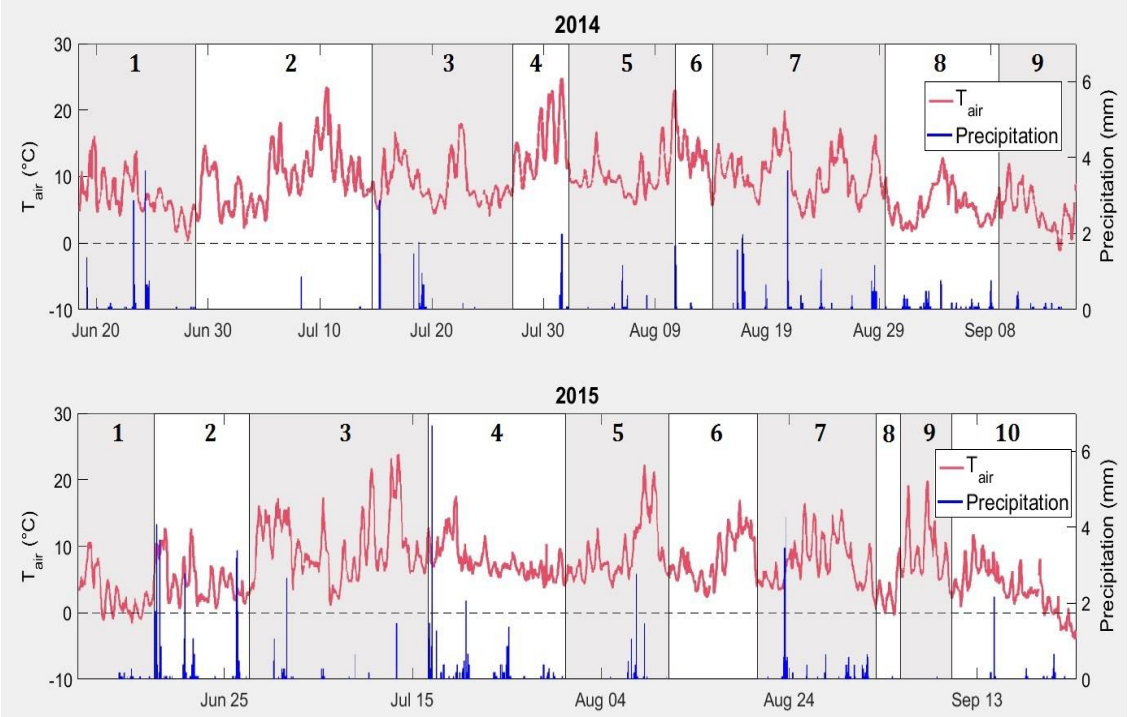

Figure 7. Subdivision measurement campaigns for small periods according to changes of the T_{air} and precipitation values. The numbers above indicate the period number.

Estimation of α coefficients and r_s was based on the solution of PM and RT approach for each *i* vegetation class using the Ordinary Least Squares (OLS) method for each allocated period. In order to achieve high accuracy of estimations, the fractions of i-class of vegetation at the footprint area (Ω_i) during the periods of observation should be taken into account (Figure 8). Due to minor fraction of 3rd vegetation class (less than 10%) at the footprint area during both measurement campaigns, the dataset from this territory were summarized with the 2nd vegetation class in order to estimate common values of α and r_s.

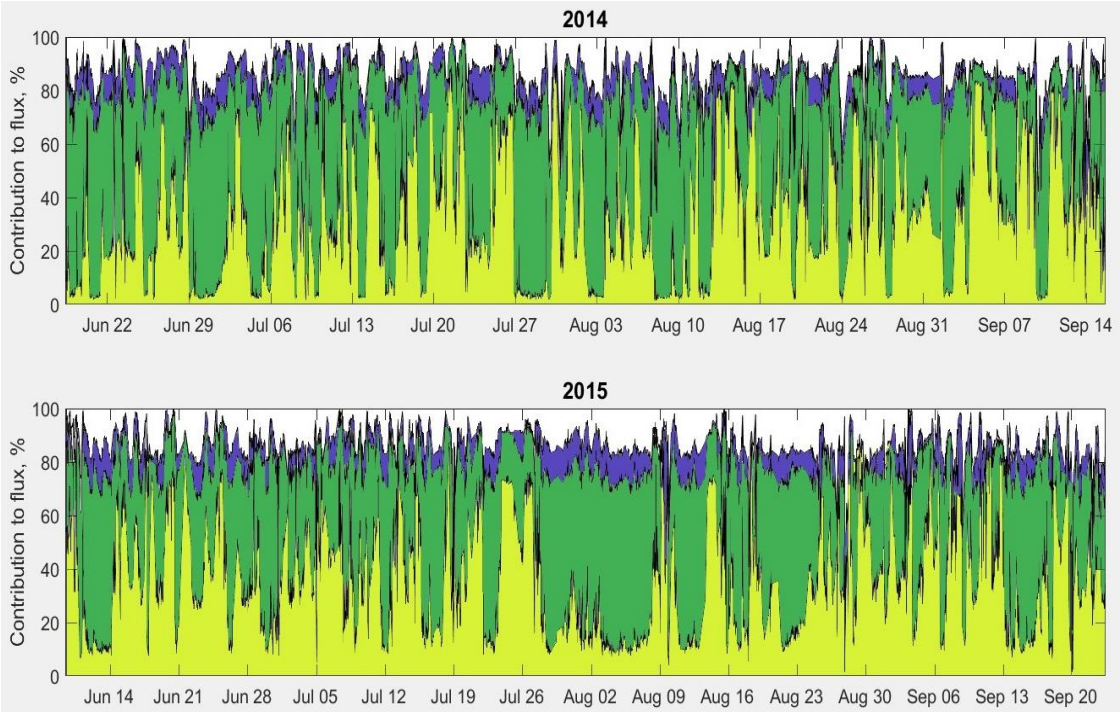

Figure 8. Contribution of vegetation classes to flux signal according to eddy covariance footprint modelling during measurement campaigns (yellow color represent 1st vegetation class, green – 2nd and purple – 3rd).

Despite the fact that over 9000 measurements were taken during the two measuring campaigns, due to quality filtering, the amount of available flux data for modeling has decreased. Thus, the amount of measurements that could be used in estimation based on the Q_GRB data amount 2839 and 3194 fluxes. For Q_GTempCorr – 3331 and 3718 for 2014 and 2015 observation periods respectively. The main reason for these differences is that for Q_GRB calculations quality of received data signals of latent and sensible heat flux signal.

4. Results

4.1. Hydrometeorological conditions

The two measuring campaigns varied greatly from each other in terms of environmental conditions. During the first measuring campaign (2014), 92.3 mm of precipitation fell, while during the 2015 campaign, it was 130.4 mm (Figure 7). Moreover, the differences can be found not only in the amount of precipitation, but at the regime of rainfall events. Thus, the largest single rainfall event during the first measurement campaign was observed on 17th August 2014 with a sum of 7.2 mm. In comparison, the rainfall night event of 23rd – 24th August 2015 clearly stands out, with a sum of precipitation close to 18 mm (Figure 9). Such long rainfall events have a serious

effect on the saturation of the active layer with water and as a consequence on fluctuations of the groundwater table position.

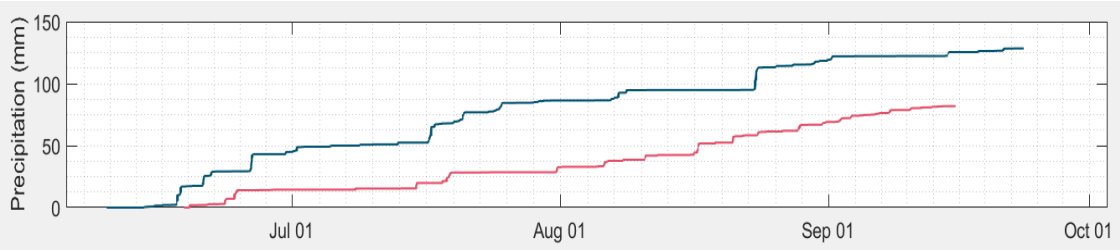

Figure 9. Cumulative precipitation data obtained at 30-min intervals during the 2014 and 2015 measurement campaigns. The red lines displays the meteorological data obtained during the 2014 measurement campaign, the blue lines.

The values of mean air temperatures, which were observed over the 2014 and 2015 measurement periods, were close to each other and were 7.7 °C and 7.1 °C, respectively (Figure 10). However, the air temperature at the start of the summer 2015 (end of May – beginning of June) was approximately 1.5 °C lower than in the previous year. The lowered temperature at the beginning of the summer season delayed snow melting and as a consequence postponed the beginning of the vegetation period.

Moreover, water level of the Lena River has a great impact on the on-going and further occurring biogeochemical processes at the flood plain. Thus, during the spring flood in 2014, the flood plain and lowest parts of the river terrace were flooded for several days, whereas 2015 only 80% of floodplain was submerged for a few hours (Rößger, 2017, unpublished).

Net radiation (R_n) varied greatly during each campaign due to the consecutive season changes, changing synoptic conditions, and the diurnal cycle (Figure 10). Thus, due to the prevalence of cloud conditions during the 2015 measuring campaign, the mean R_n value was 9% higher for the 2014 measurement campaign than for 2015. The greatest differences in R_n values in the daytime hours between the measuring campaigns were observed at the beginning of July, when the difference was close to 30%.

Based on the obtained meteorological data from Samoylov Island during 1998-2011, the average summer temperature and the sum of precipitation were 6.8 °C and 124 mm (Boike et al., 2013). Consequently, the first measurement campaign of 2014 could be characterized as a warmer and slightly drier measurement period, while the second measurement campaign of 2015 is characterized by higher mean air

temperatures and considerably higher amount of precipitation compared to the average data for Samoylov Island.

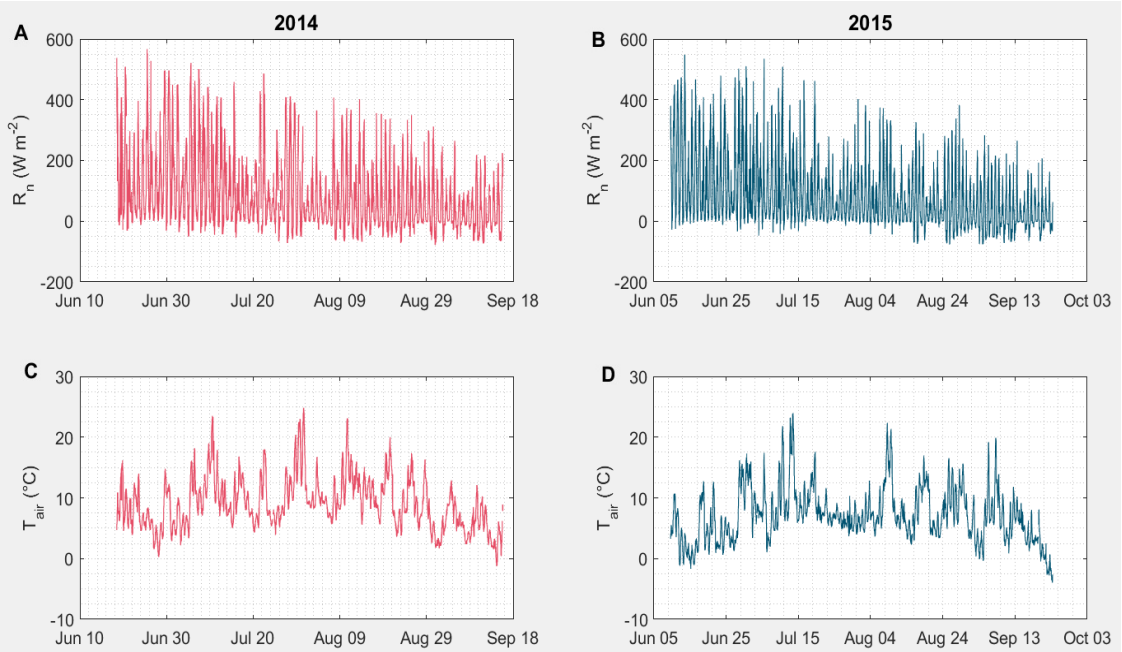

Figure 10. Overview of hydrometeorological conditions during the 2014 and 2015 measurement campaigns. The left column (red lines) displays the meteorological data obtained during the 2014 measurement campaign, the right (blue lines) - 2015. The graphs show the data obtained at 30-min intervals. A and B – net radiation (R_n), C and D – air temperature (T_{air}).

4.2. Estimation of evapotranspiration fluxes

Over 9 000 flux data measurements were taken during the two measurement campaigns: 4278 measurements were conducted over the period from 18nd June to 15th September 2014 and 5082 during the 09th June – 23rd September 2015. Subsequently, the recorded flux datasets were used to calculate the ET flux and simulate it further.

Seasonal cycles of ET and over fluxes are strongly coupled with the annual cycle of R_n. The observed ET fluxes for the 2014 and 2015 are characterized by a clearly defined seasonal trend: rising during the middle of June, peaking in the end of June – beginning of July and afterwards decreasing with varying values until September (Figure 11). Thus, maximum values during both campaigns were observed at the midday of the same day - 30th of June with the estimated amount of 0.265 mm h^{-1} and 0.26 mm h^{-1} for the first and second observation periods, respectively.

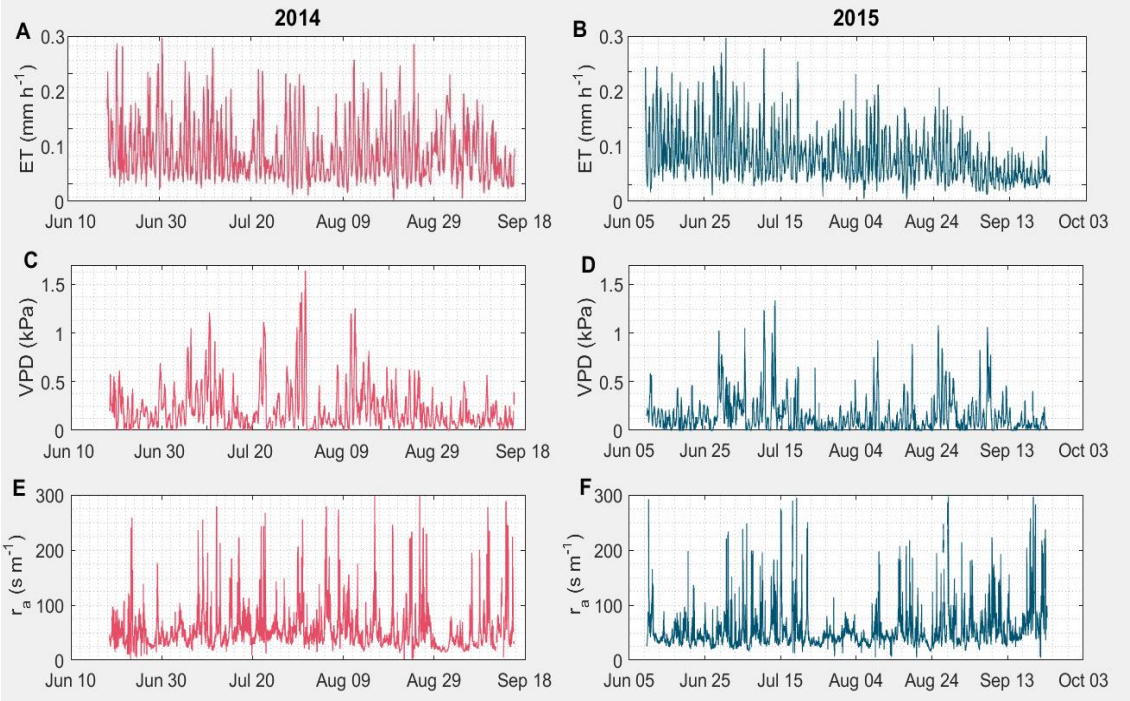

Figure 11. Estimated ET fluxes for half-hour time periods and main control factors: A and B –ET fluxes (ET), C and D – vapour pressure deficit (VPD), G and H – aerodynamic resistance (r_a). The left column (red lines) displays the recorded data during the 2014 measurement campaign, the right (blue lines) - 2015

Nevertheless, synoptic meteorological events provide a great influence on the ET flux variability. A striking example is the presence of the second peak of ET flux during the 2014 measurement campaign, which was recorded at the end of August and amounted to 0.254mm h^{-1}. As a result of the impact of an incoming cyclone, cloudy weather was established on the floodplain territory for a short period of time. This contributed to an increase of wind speed and low values of aerodynamic resistance, and as a consequence ET fluxes reached the same values as at the peak of solar insolation. Despite this, weather conditions can also have a reverse effect on the dynamics of ET flux. Precisely due to the prevalence of cloudy conditions, the rate of ET in 2015 was less than in 2014. So the mean value of ET flux for 2014 measurement campaign is 0.057 ± 0.039 mm h^{-1} (mean ± SD), while for 2015 it was 0.048 ± 0.035 mm h^{-1}.

Estimated values of aerodynamic resistance (r_a) also varied greatly over the 2014 and 2015 measurement campaigns. During both observation periods mean values of r_a were close to each other: 54.35±40.19 sm^{-1} and 54.27±22.34 sm^{-1} for the first and second observation periods respectively (Figure 11). During both measurement stages, periods of high and low values of r_a could be observed. In comparison with 2014, when

increased values were observed throughout the observation period, the dynamic change of r_a values during the second campaign looks stepwise: gradual increase in values from beginning of June until middle of July, then a rapid decline and further rising of values up to the end of measurement campaign.

Due to strong fluctuations in R_n, values of the vapour pressure deficit (VPD) also were impermanent during the two measurement campaigns (Figure 11). Based on the tight relationships between R_n and air temperature, the VPD values were significantly higher in 2014 than in 2015 (Figure 8). Recorded VPD ranged from 0 to 1.64 (mean 0.22±0.16) kPa and 0 to 1.34 (mean 0.15±0.12) kPa during the first and the second measurement campaigns. In spite of low mean values, VPD values greater than 1 kPa were observed several times during both observation periods and mainly could be linked with the diurnal cycle.

4.3. Comparison and correction of ground heat fluxes

Due to the fact that the elements of energy balance are strongly coupled with R_n, seasonal variability of ground heat fluxes could be observed during both measurement campaigns (Figure 12). For the dataset of the ground heat fluxes that were estimated as a residual term of the radiation balance equation (Q_GRB), maximum values were recorded at the daytime at the end of June and amounted 261 Wm^{-2} and 272 Wm^{-2} during the 2014 and 2015 measurement campaign respectively. During both periods of observation due to seasonal decrease of amount of incoming solar radiation, the amplitude and values of the ground heat fluxes were reduced. Nevertheless, the minimum values of the ground heat fluxes for both campaigns were recorded not at the end of the observation, but also at the end of June. Thus, the minimum value for the 2014 measuring campaign was -105 Wm^{-2}, and for 2015 – 100 Wm^{-2}. Such time closeness of the maximum and minimum values indicates extremely large daily ground heat flux variability at the beginning of observations. Moreover, the seasonal trend of decreasing amount of ground flux energy could be affected by synoptic changes. Thus, during the rainfall events and prevalence of cloudiness conditions, values of the ground heat flux were decreased. Such weather effects had a great effect on R_n during the measurement campaign of 2015. Mainly because of this, the average mean of ground heat flux during the first observation period of is almost 8% higher than for the second. Thus, this value for the 2014 observation period is - 32.86 Wm^{-2}, while for 2015 – 30.49 $Wm^{-2.}$

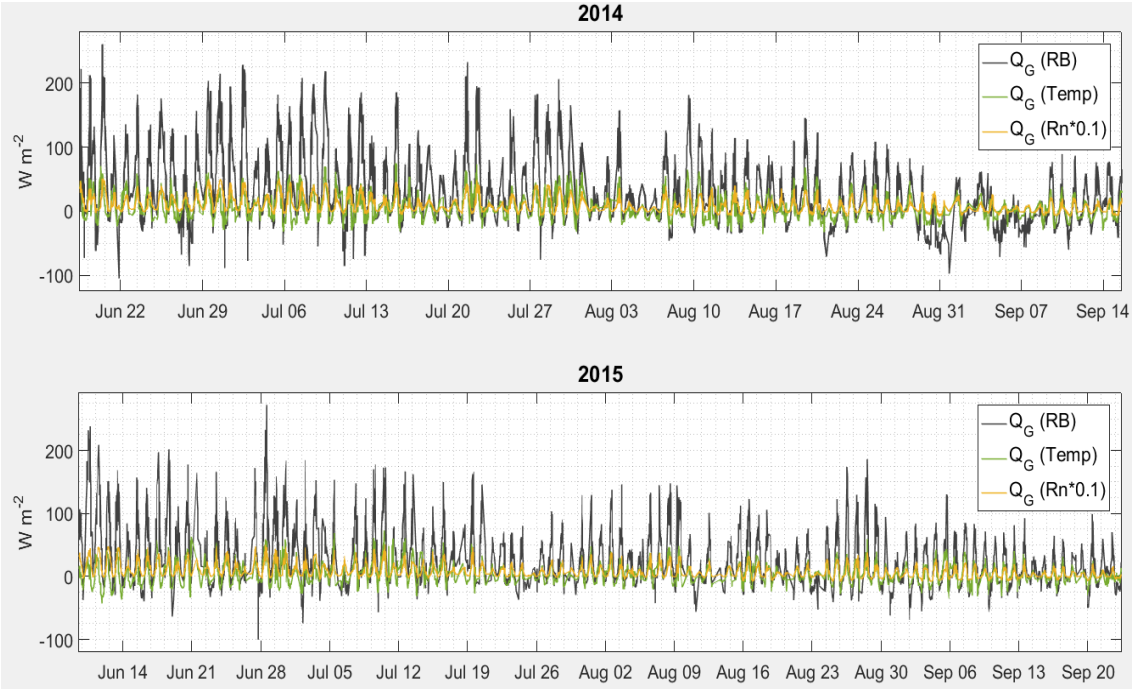

Figure 12. Differences between the values of ground heat fluxes, calculated as the residual term of the radiation balance equation (Q_GRB), based on soil temperature data (Q_GTemp) and as relative fraction of net radiation (Q_GRn*0.1)

Values of ground heat fluxes, calculated based on the soil temperature data (Q_GTemp), have similar to Q_GRB values seasonal variability. Nevertheless, the mean values of Q_GTemp are more than 4 times lower than mean values of Q_GRB and amounted 6.9±15.9 Wm^{-2} and 4.82±13.4 Wm^{-2} for 2014 and 2015 measurement campaign respectively. Moreover, in comparison with the Q_GTemp, biggest values during both observation periods were recorded not at the period of maximum solar insolation, but at the middle of July and are closed to the 75 Wm^{-2}. However, minimum values of Q_GRB were recorded at the begging and end of summer for the first and second measurement campaign respectively.

Moreover, figure 8 clearly shows close relationship between values of Q_GTemp and values of ground heat flux estimated as relative fraction of R_n values (Q_GRn*0.1). Furthermore, figure 8 displays striking difference between values of Q_GTemp, Q_GRn*0.1 and Q_GRB. Nevertheless, the obtained data of Q_GTemp and Q_GRB are characterized by a co-directional change and a similar dynamics. Thus, the correlation coefficient between Q_GRB and Q_GTemp for 2014 and 2015 measurement campaign is high and is estimated 0.732 and 0.694 respectively (Figure 14). Based on this, as well as high correlation, coefficients between the datasets and the similar dynamics changes for

both measurement campaigns, the values of Q_GRB and Q_GTemp were used to find the correction coefficients between them (Figure 13, Appendix, Table 1).

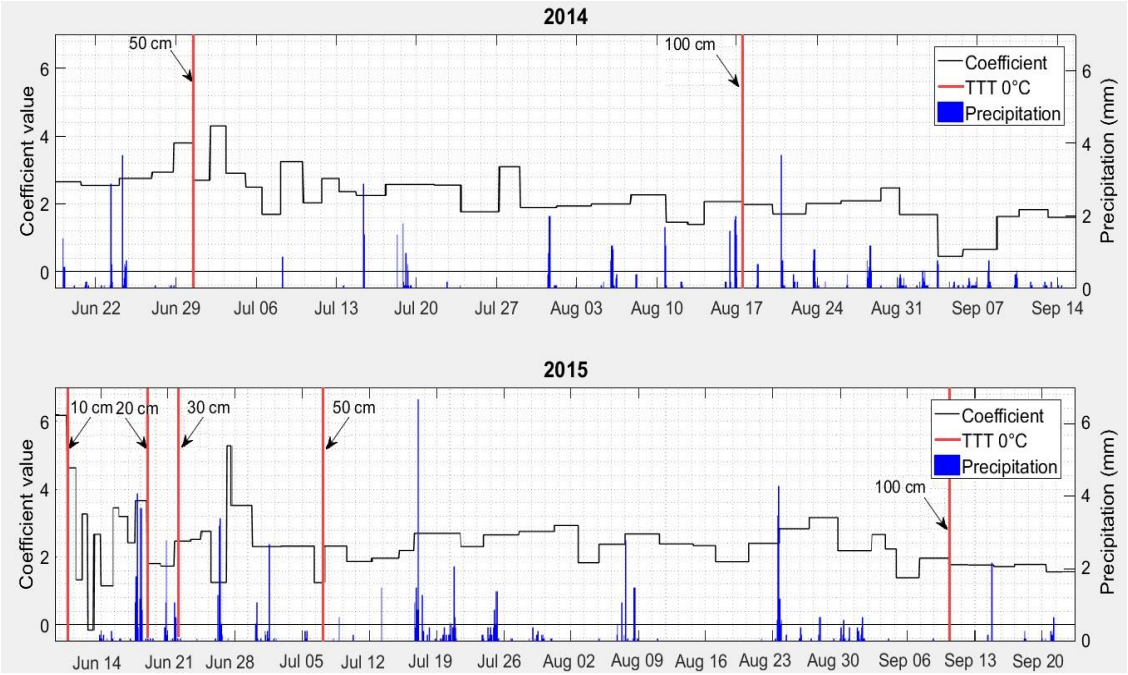

Figure 13. Change of the ratio between values of Q_GRB and Q_GTemp during the measuring campaigns of 2014 (upper graph) and 2015 (lower graph). The blue indicators show the amount of precipitation in mm that fell in the half-hour observation period. Red lines - temperature transition through 0°C at depths of temperature measurement. On the side of each line the depth is indicated at which the transition was recorded through 0°C.

Thus, for both measuring campaigns, the trend of seasonal correction coefficient changes looks similar: high values, which were calculated for the beginning of the seasons, gradually decreased towards the end. Nevertheless, maximum values of correction coefficient were estimated for different periods of June and differ from each other. During the 2014 measurement campaign, the maximum value of correction coefficient was estimated at 4.29 and was recorded for the period between 30th of June and 1st of Jule, while for 2015 – 6.17 exactly at the beginning of observation from the 10th -11th of June. Moreover, the mean values of correction coefficient were lower for the summer of 2014 than 2015 and amounted 2.23 and 2.42 respectively. Despite of this, at the end of both periods of observation value of correction coefficient was less than 2. It is also worth noting the sharp jumps of coefficient values in the direction of larger and smaller values during both periods of observation.

Additionally, cross-correlation analysis was done in order to correct Q_GTemp dataset. Cross-correlation function for each parameter has only one maximum, providing that the correlation between the measurements exists. Thus, for both measurement campaigns a time lag between pair Q_GTemp - Q_GRB of 30 minutes interval (1 period of observation) was found. These delays could be linked with the propagation of the thermal wave in the soil masses and subsequent later recording by measuring instruments. After the procedures to correct the Q_GTemp data were taken, the correlation between the Q_GRB and Q_GTempCorr increased to 0.789 and 0.783 for the measuring campaigns of 2014 and 2015, respectively (Figure 14).

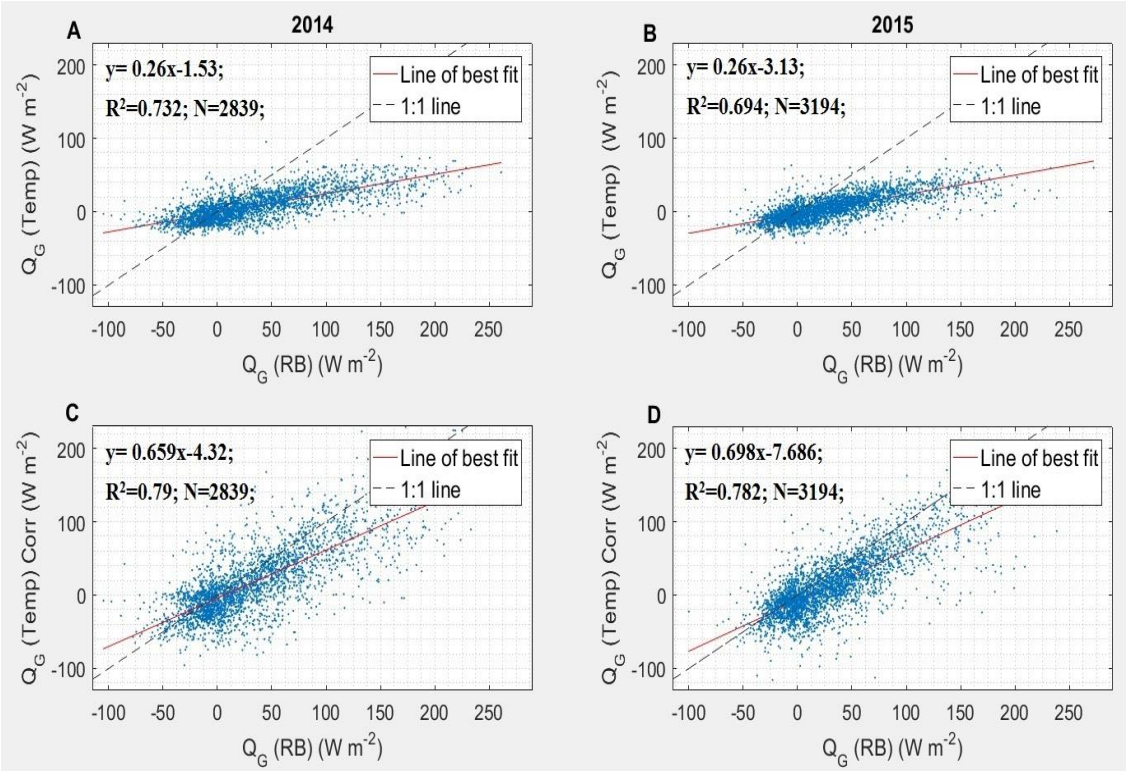

Figure 14. Scatter plot of Q_GRB and Q_GTemp before correction for the time lag and correction factor (A and B) and after corrections Q_GTempCorr (C and D). Line of best fit was found by ordinary least squares (OLS) regression.

4.4.Priestly-Taylor parameters for vegetation classes

Dynamic changes of α coefficients during two observation campaigns are shown in figure 15. According to calculated results, the α coefficient for the 1st vegetation class dynamic pattern is close to the bell-shape form. Both observation periods have pronounced seasonal variation cycles: rising up to the end of July, peaking at the beginning and middle of August and further gradually decreasing up to the end of September. Thus, maximum α coefficient values for 2014, which was estimated based

on the Q_GRB, was estimated for the middle of August and amounted 1.354±0.156 (mean ± SD). For Q_GTempCorr dataset maximum α coefficient value was observed at the beginning of August – 1.181±0.182. The minimum α parameter values were estimated for middle of September for both databases – 0.3459±0.207 and 0.2065±0.182 for Q_GRB and Q_GTempCorr, respectively (Appendix, table 2,4,6,8).

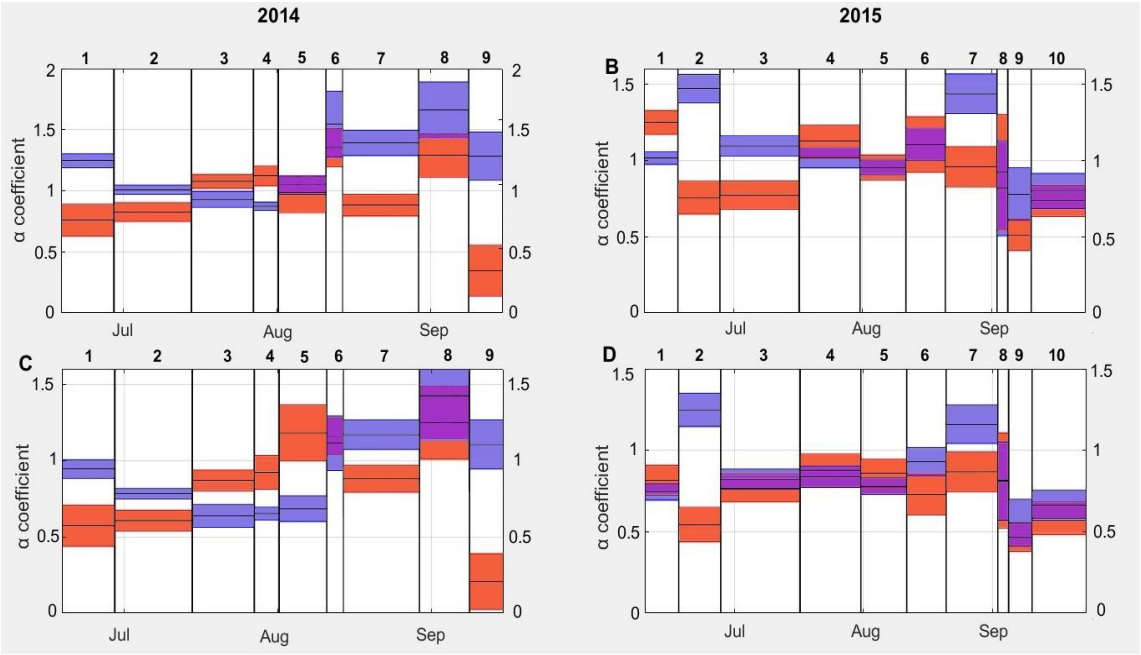

Figure 15. Dynamic change of α coefficients during two measurement campaigns (2014 - left column, 2015 - right). Red color represents 1st vegetation class, blue - combined 2nd and 3rd vegetation class. The width of the line indicates the value of standard deviation. Purple color displays areas where standard deviations for each vegetation class overlap each other. On the graphs A and B, calculations were based on the Q_GRB dataset, while C and D - on the Q_GTempCorr dataset. The numbers above indicate the period number.

For 2015 summer campaign α coefficient dynamic changes of 1st vegetation class also could be referred as close to the bell-shaped. However, this distribution pattern is slightly broken by high values of α coefficient estimated for the beginning of the measurement campaign. Thus, maximum α coefficient values for 2015 for Q_GRB database were recorded in the middle of June and amounted 1.248±0.077. Despite this, the maximum α parameter values for 2015 for Q_GTempCorr dataset was estimated for the second half of July – 0.8755±0.1011. Minimum values as at the previous measurement campaign were obtained in the second half of September: 0.5112±0.1018 and 0.467±0.0865 for Q_GRB and Q_GTempCorr respectively. In addition, it should be

noticed that estimations based on the Q_GRB dataset allowed obtaining higher values of α coefficient during both observation periods then Q_GTempCorr. Hence, the mean values of α coefficient for the 1st vegetation class based on the Q_GRB data were 0.9305±0.1846 and 0.9108±0.1647, while for Q_GTempCorr dataset 0.8284±0.2355 and 0.7457±0.1103 for 2014 and 2015 observation periods, respectively (Appendix, table 2,4,6,8).

During the 2014 measurement campaign, the dynamic of combined 2nd and 3rd vegetation class changes are wave-like. Values of α coefficient for combined 2nd and 3rd vegetation class were decreasing up to the end of July with further gradually rising up to the beginning of September. The minimum α coefficient values were observed at the end of July for both databases – 0.8737±0.0325 and 0.637±0.0735 for Q_GRB and Q_GTempCorr respectively. Maximum α coefficient values were calculated at the begging of September and amounted – 1.662±0.228 and 1.426±0.291 for Q_GRB and Q_GTempCorr datasets respectively.

The distribution of α coefficient values during the 2015 measurement campaign also could be classified as close to wave, but with a higher frequency. Over the summer of 2015 several periods with local maximum and minimum value were established. Based on both database calculations, maximum values were observed during the first α coefficient peak 1.469±0.092 and 1.248±0.101 for Q_GRB and Q_GTempCorr datasets respectively. At the same time, minimum values were calculated for the final values decreasing 0.7779±0.1719 and 0.5556±0.1426 for Q_GRB and Q_GTempCorr databases. As at the case of 1st vegetation class values, α coefficient estimations that were based on the Q_GTempCorr data for combined 2nd and 3rd vegetation class obtained lower mean results than by using Q_GRB: 1.2049±0.2162 and 1.0794±0.168, while 0.9406±0.2287 and 0.8699±0.1509 for 2014 and 2015 observation periods, respectively. Based on the obtained results, estimated α coefficient values for the 1st vegetation class were lower than for the combined 2nd and 3rd vegetation class.

Based on the estimated α coefficient values for each period ET fluxes were modeled. Thus, estimations that were based on the Q_GRB dataset allow receiving high values of coefficient of correlation (R^2) – 0.92 and 0.932 for 2014 and 2015 campaigns receptively (Figure 16). Calculations that were maintained on the Q_GTempCorr database held R^2 values as 0.834 and 0.86 for 2014 and 2015 observation periods.

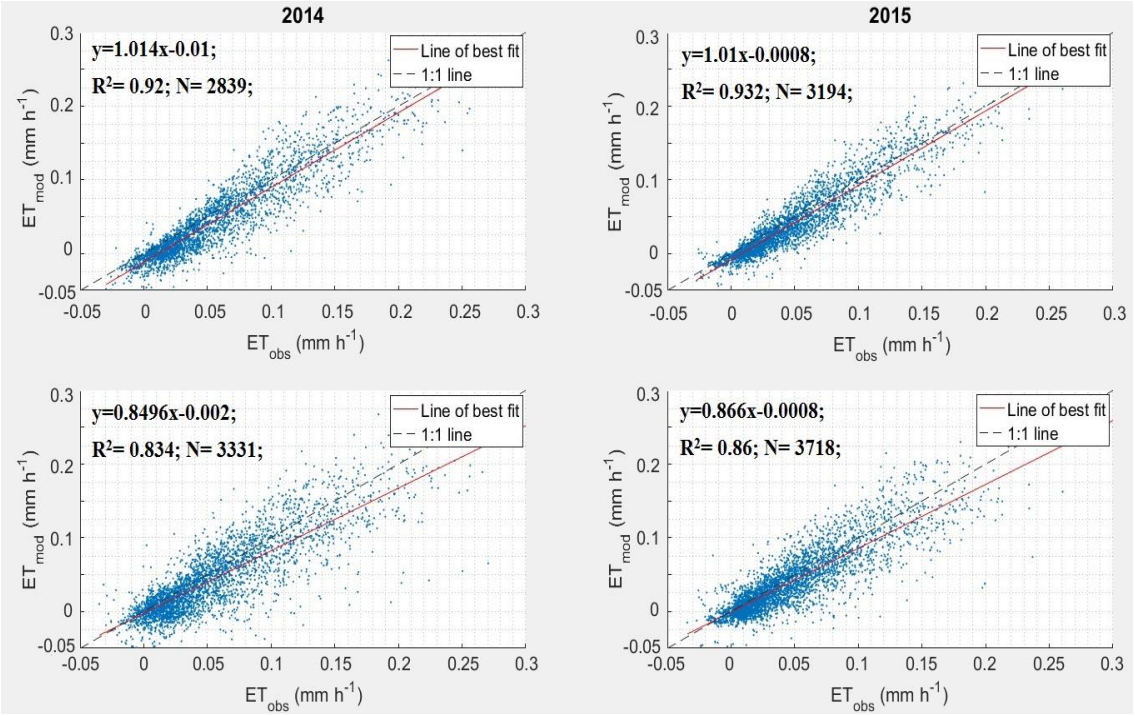

Figure 16. Scatter plot of observed ET (ET_obs) and modelled ET (ET_mod) based on the obtained α coefficient. Calculations on the graphs A and B were based on the Q_GRB dataset, while C and D - on the Q_GTempCorr dataset. Line of best fit was found by ordinary least squares (OLS) regression.

4.5. Surface resistances estimated for vegetation classes

Dynamic change of r_s values during two measurement campaigns are demonstrated in figure 17. For the first observation period, the obtained results are characterized by a great variability over the campaign. Maximum r_s values for 1st vegetation class were obtained for the first half of July and amounted 193.6±30.5 sm^{-1} and 216.4±36.5 sm^{-1} for Q_GRB and Q_GTempCorr datasets respectively. The minimum values were found at the beginning of September and were 75.84±12.34 sm^{-1} for Q_GRB and 72±13.2 sm^{-1} for Q_GTempCorr databases (Appendix, table 3,5,7,9).

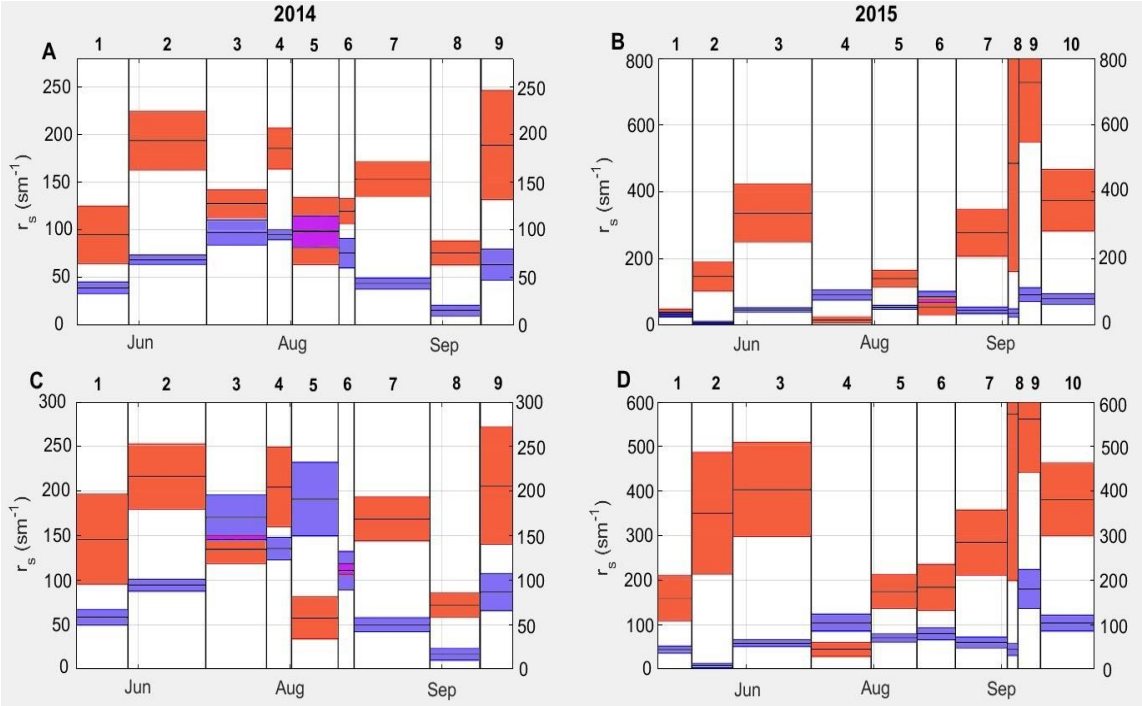

Figure 17. Dynamic change of r_s during two measurement campaigns (2014 - left column, 2015 - right). Red color represents 1st vegetation class, blue – combined 2nd and 3rd vegetation class. The width of the line indicates the value of standard deviation. Purple color displays areas where standard deviations for each vegetation class overlap each other. On the graphs A and B, calculations were based on the Q_GRB dataset, while C and D - on the Q_GTempCorr dataset. The numbers above indicate the period number.

The two measurement campaigns differed greatly from each other in terms of obtained r_s values for 1st vegetation class. For the second observation period, distribution of obtained r_s values over the campaign could be classified as a clear step-like. Thus, values raise up to the middle of July, fall at the second half of July and reach a second peak during the measurements in middle of –September. Exactly at the second seasonal peak, maximum values of r_s could be founded: 727.6±177.3 sm^{-1} for Q_GRB and 573.7±374 sm^{-1} for Q_GTempCorr databases. Minimum of r_s occur in the period of rapid decline - 16.09±8.51 sm^{-1} for Q_GRB and 44.38±15.39 sm^{-1} for Q_GTempCorr datasets. Furthermore, the mean values calculated for 1st vegetation class during two measuring campaigns differ greatly from each other. While the mean values for Q_GRB database are 138.7 ±37.60 sm^{-1} and 227.9±151.52 sm^{-1}, for Q_GTempCorr database these values are 149.88±45.01 sm^{-1} and 282.58±124.39 sm^{-1} for 2014 and 2015 measurement campaigns respectively (Appendix, table 3,5,7,9).

According to calculated r_s values for combined 2nd and 3rd vegetation class during the 2014 observation period distribution pattern is close to the bell-shape form. Thus, observation period has pronounced cycle over the seasons: rising up to the end of July, peaking at the beginning and middle of August and further gradually decreasing up to September. Nevertheless, at the end of measurement campaign, a second peak is observed. Thus, maximum r_s values during the 2014 measurement campaign were estimated for the end of July and first days of August – 98.11±16.49 sm^{-1} for Q_GRB and 191 ±41.2 sm^{-1} for Q_GTempCorr databases. For the same observation period minimum values were obtained during the first part of September - 15.56±5.37 sm^{-1} for Q_GRB and 16.57 ±6.41 sm^{-1} for Q_GTempCorr datasets. Mean values of r_s for combined 2nd and 3rd vegetation class for 2014 were equal 63.51 ±23.31 sm^{-1} when Q_GRB data was used in computations and 96.89 ±46.13 sm^{-1} when Q_GTempCorr was used.

The distribution of estimated r_s values for combined 2nd and 3rd vegetation class during the 2015 measurement campaign also looks like a bell. Nevertheless, in 2015 the second peak of r_s values was clearly pronounced. Thus, for the middle of September were computed maximum values for Q_GRB and Q_GTempCorr datasets: 92.44±19.96 sm^{-1} and 180.3±43.5 sm^{-1} respectively. For the same observation period minimum values were founded for the second half of June and obtained results were close to each other: 7.01 ±4.35 sm^{-1} based on the Q_GRB and 7.64±4.69 sm^{-1} for Q_GTempCorr. Mean values of r_s for combined 2nd and 3rd vegetation class for 2015 was estimated as 57.88 ± 22.81 sm^{-1} when Q_GRB data was used in computations and 73.69 ±27.93 sm^{-1} when Q_GTempCorr was used.

As with the obtained α coefficient values, r_s values were used in modeling of ET fluxes for each period. Moreover, as in the case with α coefficient, calculation that were based on the Q_GRB dataset allow to receive high values of R^2 – 0.879 and 0.9035 for 2014 and 2015 campaigns receptively (Figure 18). Calculations that were established using the Q_GTempCorr database yielded values of coefficient of R 0.791 and 0.8021 for 2014 and 2015 observation periods.

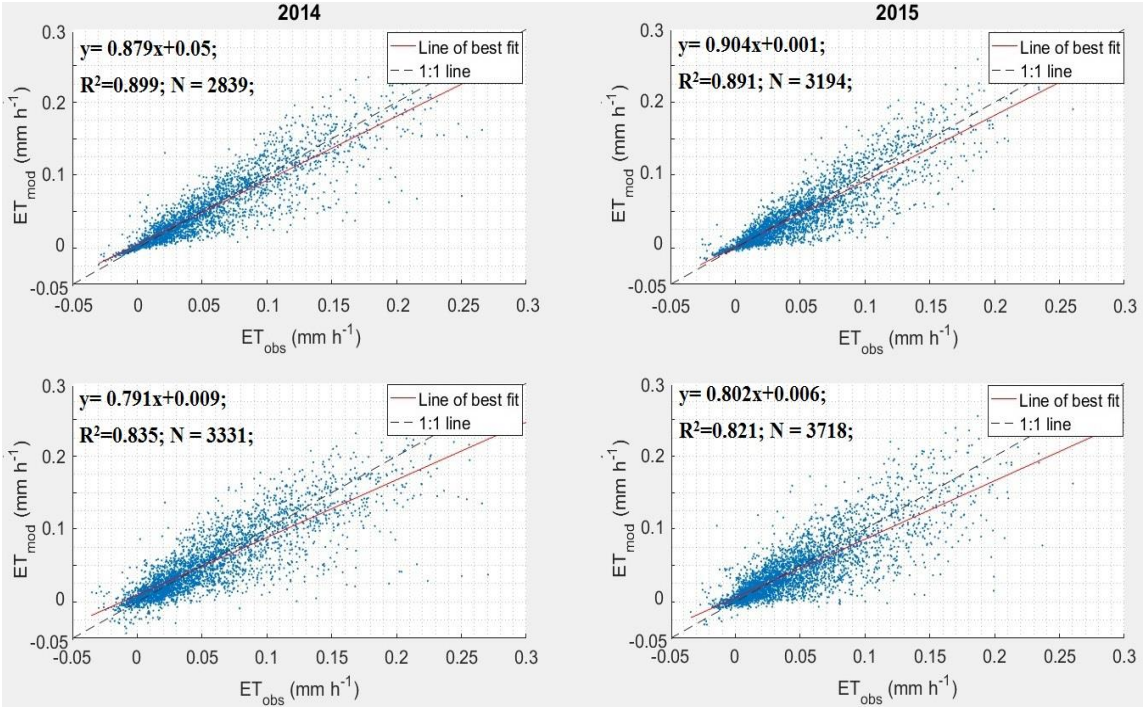

Figure 18. Scatter plot of observed ET (ET_obs) and modeled ET (ET_mod) based on the obtained r_s values. On the graphs A and B, calculations were based on the Q_GRB dataset, while C and D - on the Q_GTempCorr dataset. Line of best fit was found by ordinary least squares (OLS) regression.

4.6. Spatial variability of modeled evapotranspiration fluxes

In order to evaluate the spatial heterogeneity of ET fluxes at the floodplain area, it is necessary to use the best modeled values. For this purpose, for each observation campaign, a range consisting of the best modeled values of ET was formed. The criterion for the range forming was the estimated value of the determination coefficient (R^2_{adj}) obtained during the calculation of ET by the PT and PM methods. It should be emphasized that values of the R^2_{adj} obtained during the calculations based on Q_GTempCorr were significantly lower than based on Q_GRB. As a result, the modeled values based on Q_GTempCorr were not used in the compilation of the series. Thus, the series of the best-simulated values are half-formed by the values obtained by PT and PM approaches (Table 1)

Table 1. Approaches of ET calculation allowed obtaining the best modeled results (by periods). The abbreviation denotes the values of the method that was used in the compilation of the series (PT – Priestley-Taylor, PM – Penman- Monteith).

2014	Date	18.06 - 28.06	28.06 - 14.07	14.07 - 27.07	27.07 - 01.08	01.08 - 10.08	10.08 - 14.08	14.08 - 29.08	29.08 - 08.09	08.09 - 15.09	
	Period	1	2	3	4	5	6	7	8	9	
	Approach	PT	PT	PT	PM	PT	PM	PM	PM	PM	
2015	Date	09.06 - 17.06	17.06 - 27.06	27.06 - 16.07	27.07 - 31.07	31.07 - 11.08	11.08 - 20.08	20.08 - 02.09	02.09 - 04.09	04.09 - 10.09	10.09 - 23.09
	Period	1	2	3	4	5	6	7	8	9	10
	Approach	PT	PT	PT	PT	PT	PM	PT	PM	PM	PM

Due to the fact that the modeling of ET fluxes for different vegetation classes was based on comparison with already estimated ET fluxes, their combined dynamics repeats the already described dynamics of changes in ET fluxes over the seasons. Nevertheless, some differences between the calculated ET values for different vegetation classes at the footprint area could be observed (Figure 19). Thus, the dynamics of the change in ET values for both vegetation classes represents a gradual decrease in values with small fluctuations during the seasons.

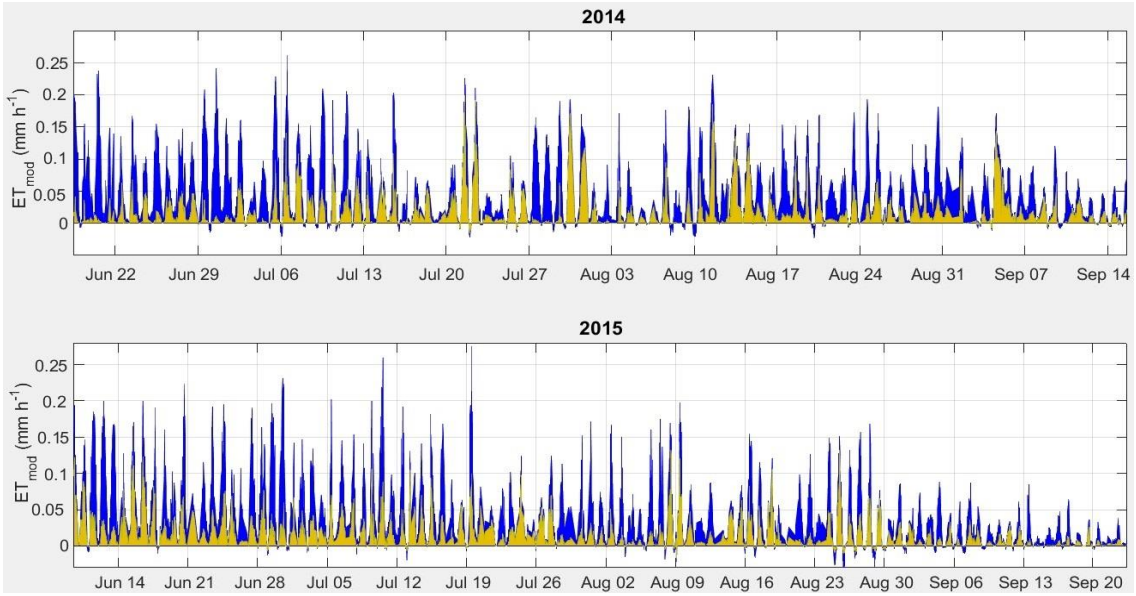

Figure 19. Decomposed ET fluxes calculated for footprint area for two vegetation classes over the 2014 and 2015 measurement periods. Yellow color describes the 1st vegetation class, blue - combined 2nd and 3rd vegetation classes.

According to the obtained results, the combined 2nd and 3rd vegetation class is a major contributor of ET. Thus, during the first measurement campaign the fraction of the combined 2nd and 3rd vegetation class from the total modeled ET values for the fetch is 67%, while for the second – 65%. Nevertheless, the greatest differences in values over the season could be observed exactly for combined 2nd and 3rd vegetation class. Thus, for 2014 measurement campaign the mean combined 2nd and 3rd vegetation class is 0.035±0.04 mm h^{-1}, while for the 2015– 0.019±0.339 mm h^{-1}. In comparison, mean value for the 1st vegetation class for both observation campaigns is not characterized by such a strong variability. Thus, for the first measurement campaign, the mean value for 1rd vegetation class is 0.017±0.002 mm h^{-1}, while for the 2015 – 0.015±0.003 mm h^{-1}.

The significant variability of ET fluxes for both vegetation classes is the result of constant wind direction changes and, as a consequence, the dimensions of the footprint area. Due to the spatial heterogeneity of distribution of vegetation classes on the floodplain territory, the footprint area during each observation period consists of territories where the ET process is actively going and the areas where this process is slow. Their approximate distribution around the EC tower becomes evident, depending on the direction of the wind and the fractions of the *i*-class of vegetation at the footprint area (Figure 20). Thus, during both measurement campaigns, little ET fluxes were recorded during the periods of northern and eastern winds prevailing, where the 1st vegetation classes and combined 2nd and 3rd vegetation class are situated respectively. On the contrary, when the wind came from northwest, northeast and southeast directions, when at the fetch prevail combined 2nd and 3rd vegetation class, but fraction of the 1st vegetation is also high, maximum values of ET fluxes in the range of 0.07 – 0.13 mm $30min^{-1}$were observed.

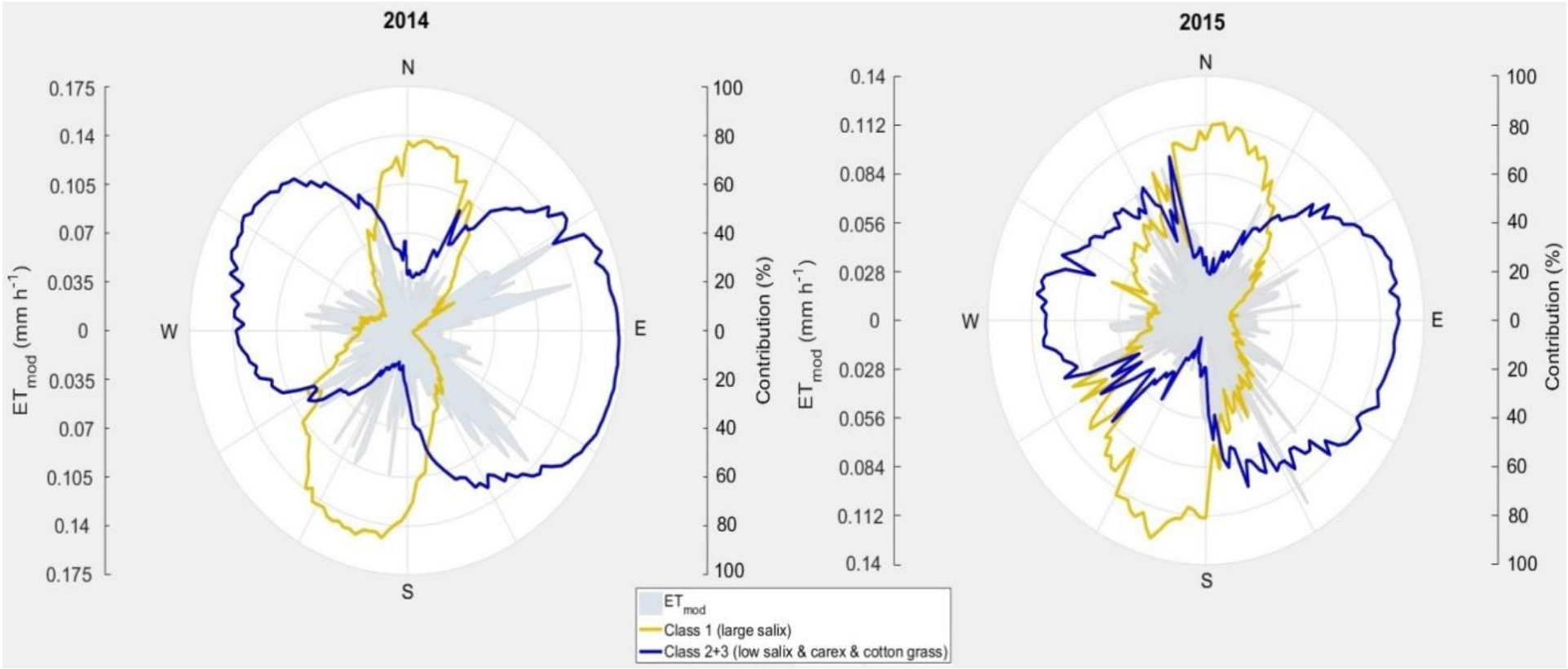

Figure 20.Wind direction dependencies of ET fluxes and their vegetation class contributions for both measurement campaigns 2014 and 2015 sorted by 2° wind direction bins. Negative values removed.

Moreover, modeled results allow removing from the calculations influence of fraction of each vegetation classes at the footprint area and obtaining rates of ET from 1 square meter (Table 2). Nevertheless, because of the ET rates decrease at the end of the observation periods, it is not possible to correctly identify the parameters for the ET model decomposition. As a result the ET rates for the each vegetation classes from 1 square meter could be used only from the beginning of observations to the end of August. According to the obtained results, the total ET rates for the 1st vegetation class during the both measurement campaigns were close to each other – 41.5 mm and 35.2 for the first and second observation periods respectively. Nevertheless, only during the second half of June, ET rates for the 1st vegetation class for 2015 were higher than 2014. A similar situation was observed for ET values for the combined 2nd and 3rd vegetation class. Thus, obtained ET rates over the whole second measurement campaign were lower than estimated for the first observation period. This led to that the total amount of water that evapotranspirated from the territories of 2nd and 3rd vegetation classes during the first observation period is 1.36 times higher than during the second: 90.6 mm and 66.6 mm for the 2014 and 2015 measurement campaigns respectively. Moreover, calculated results allow estimating mean daily values of ET from the each vegetation classes. Thus, during the summer period between July 21 – August 21 the daily ET rates for the 1st vegetation classes were: 0.6±0.26 mm/day and 0.4±0.21 mm/day and for the combined 2nd and 3rd vegetation class: 1.05±0.42 mm/day and 0.75±0.3 mm/day during the first and second measurement campaign respectively.

Table 2. ET rates from 1 m^2 for each vegetation class and amount of precipitation for 1 m^2 for over the 2014 and 2015 measurement campaigns.

Period		18.06.–30.06.	01.07.-31.07.	01.08.-31.08.	18.06. -31.08.
2014	1st (mm)	4.56	19.08	17.81	41.5
	2+3rd (mm)	24.34	35.53	30.72	90.6
	Precipitation (mm)	14.5	18.1	36.5	69.1
2015	1st (mm)	7.34	15.91	11.91	35.2
	2+3rd (mm)	18.06	26.21	22.32	66.6
	Precipitation (mm)	34.8	41.5	32.9	109.2

5. Discussion

5.1. Influence of ground heat flux models on the evapotranspiration estimates

Due to the fact that the resistance between the R_n and Q_G is a key driver for such methods of evapotranspiration calculations as PT and PM, the importance of their accuracy cannot be underestimated. According to Foken [2008], during most EC experiments and observations the sum of R_n and Q_G is often considerably larger than the sum of turbulent fluxes. As stated in previous investigations, the error in estimations of Q_G as a residual term from the energy balance equation can reach 5-20% of calculated value (Foken, 1998).

Due to the lack of investigations of Q_G at the floodplain area, obtained values could be compared only to values recorded at another geomorphological unit of the Samoylov Island, the part that is composed of sediments of a Holocene river terrace. Compared to the results of the 2003/2004 measurement campaigns on the Holocene river terrace, the average values obtained at the modern floodplain during the summer periods (June 11 – August 31) of 2014/2015 were approximately 2 times higher (Kutzbach, 2006).

As an alternative method to Q_GRB calculation, an approach that was based on the soil temperature data measured at different depths was used (Rusin, 2014). Obtained results (Q_GTemp) are close to the values of control method, which is based on the R_n (Q_GRn*0.1). Nevertheless, the results obtained by approaches mentioned above are strikingly different from the results of Q_GRB calculation (Figure 12). However, these alternative techniques have either not been applied, as in the case of Q_GTemp, and require additional calibration or improved consideration of permafrost-affected, arctic environmental conditions at the study site, as in the case of Q_GRn*0.1.

One of the main reasons that prevented from obtaining values as Q_GTemp close to Q_GRB was the lack of dynamic change data of the soil volumetric heat capacity value during the measuring campaigns. The volumetric soil heat capacity is one of the most important thermodynamic parameters that affect on-going thermodynamic processes. The volumetric heat capacity of the soil is summed up as the sum of the volumetric heat capacities of all major components of the soil (ice, organic matter, starting material, water and other aqueous solutions, air and gases), taking into account the fraction of each element in the total volume of the soil (Farouki, 1986). A considerable variability

of these parameters during the season in high-latitude environmental conditions is caused by frequent transitions of soil elements from one phase state to another (for example, from ice to water) and hindered water infiltration through the soil and redistribution of soil water due to the presence of a waterproof layer of permafrost (Fröb, 2011). However, due to the lack of soil properties data that were available in the original investigation conducted in temperate climate conditions, the value of volumetric soil heat capacity was assumed as 0.38 cal cm^{-3} s^{-1} (Rusin, 2014).

We assumed that the variability of Q_GRB was partly due to changing volumetric heat capacity of the floodplain soil. Due to the fact that the observations were conducted with the time interval of half an hour, the volatility of this coefficient was taken into account. The correction coefficient was calculated on the basis of the ordinary linear equation Q_GRB = Coeff * Q_GTemp for each period of observation (Figure 13, Appendix, table 1). In order to take the variability of volumetric soil heat capacity into account during the periods of observation and obtain a high accuracy results, values of correction coefficient were estimated for intervals of 1-3 days. Particular attention was paid to periods with rainfall events and time of temperature transitions through 0 °C at different soil depths.

Changes of correction coefficient during the measurement campaigns could be linked with two factors. Firstly, due to the fact that the Q_GRB in comparison with the Q_GTemp is more susceptible to amount of energy, that reached the ground, exactly at the beginnings of the measurement campaigns, maximum values of correction coefficient were obtained. Due to the seasonal changes, the influence exerted by R_n decreased, which affected the dynamics of the correction factor. Another factor that has a direct temporary effect on the volumetric soil heat capacity, and as a consequence, the correction coefficient is the amount of water in the soil pore space. Due to the high water volumetric heat capacity (4.2 kDJ dm^{-3} $°K^{-1}$), increasing the amount of water in the soil affects the increase in the volumetric heat capacity of the entire soil volume. Fluctuations of water amount in the soil could be associated with two factors: rain events and thawing of permafrost. Probably, rapid increases of correction coefficient value occurred during the periods of active thawing of frozen ground in the top soil and heavy rains. However, due to the seasonal thawing of permafrost and opening of routes for the removal of surplus water from the soil, the impact of such events on the value of the correction factor for the campaigns probably decreased over the summer season.

5.2. Estimation of evapotranspiration fluxes in heterogenous tundra conditions by Priestly-Taylor and Penman- Monteith approaches

5.2.1. Changing of alpha coefficient values during the measurement campaigns

The key factor of successful use of PT method for modeling the ET is the estimation of the best value α coefficient. According to the Priestley and Taylor hypothesis, for areas that are almost covered by low vegetation and characterized by an unlimited amount of available water for the ET process, the value of the α coefficient is close to the 1.26 (Priestley and Taylor 1972). However, a lot of successful studies comprehended that the α coefficient value is not constant and its deviations are strongly depend on the conditions of soil moistening (Flint and Childs, 1991; Stannard, 1993), vegetation type (Viswanadham et al., 1991, De Bruin and Holtslag, 1982) and its height (McNaughton and Black, 1973).

Dynamic changes of α coefficient values for 1st vegetation class estimated on both datasets of ground heat fluxes look very similar during the measurement campaigns (Figure 15). Because shrubs are represented in elevated areas of floodplain area, the fluctuation of amount available soil moisture is not so high. Thus, bell shape form of α coefficient values changes could be a good marker of seasonal vegetation cycle. Nonetheless, based on this fact, that the stage of phenological development of plants and transpiration properties mainly influence the α coefficient values for the 1st vegetation class, during periods, when the necessary conditions of PT approach is not totally applied, increased values of α coefficient values for 1st vegetation class could be observed. For example, due to high values of r_a or VPD, which were recorded at the end of July 2014 (4 period) and in the middle of August 2014 (6 period), value of the α coefficient, calculated on the base of Q_GRB data, was also increased.

Dynamic changes of α coefficient values for the combined 2nd and 3rd vegetation classes estimated on both datasets of ground heat fluxes during the measurement campaigns look close to a wave form (Figure 15). In comparison with the 1st vegetation class, 2nd and 3rd refer to the transitional areas between elevated parts of floodplain and actually wet depression areas. Due to the fact that these territories represent a weakly drained zone, the soil is always over and high saturated with water over the whole observation campaign. Moreover, in this study the similar feature of dynamic changes of α coefficient values for the lowlands territories were observed as at

many places over the Arctic (Hobbie, 1980). Thus, highest values are linked with the large amount of water formed as a result of snow melting with the subsequent oversaturation of the upper almost non-thawed layer of soil. During these periods, the evaporation processes from these areas are not restricted, and elevated values of α coefficient are obtained. Meanwhile, during the campaigns, the α coefficient value decreases due to the gradual evaporation of water from these areas, as well as thawing of the upper permafrost layer, and as a consequence redistribution of surplus of groundwater. Also, it`s necessary to underline, that obtained high values for the 1st and combined 2nd-3rd vegetation classes at the begging of measurement campaigns have different dynamics. While for the 2014 observation period the described above scenario, during the 1st and 2nd allotted periods could be observed alternate attainment of peak values for each vegetation classes. This variation could be linked with the delayed beginning of snowmelt and ice thawing due to that in early summer of the 2015 air temperatures was around 1.5 °C colder than the previous year.

The α coefficient dynamic over the summer is linked with the slow decrease of available soil moisture and the passage of all phenological stages from germination to senescence by plants. Nevertheless, even at the end of observation periods such factor as rain fall events (especially heave), can have a significant effect on the increase in the values of the α coefficients for both classes (Figure 9). A striking example of this thesis is the rapid increase of α coefficient values for 1st and combined 2nd-3rd vegetation classes at the beginning of September 2014 (8 period) and the second half of July 2015 (4 period).

Plants reach the limits of their development and growth at environmental conditions of Arctic in late July - early August (Tieszen, 1978). According to the previous studies and experiments, α coefficient values of well-drained territories that provide best growing conditions for sedge tussocks, lichens and shrubs is close to 1.00 (α = 0.95, Rouse and Stewart, 1972; α = 1.00, Stewart and Rouse, 1976). While for the wet lowlands characterized mainly by wet sedge, investigations found that α coefficient value should be close to 1.26 at the end of July (α = 1.26, Stewart and Rouse 1976; α = 1.3, Roulet and Woo 1986; 1990; α = 1.3, Rovanesk et al., 1996). If we will take into account that estimated α coefficient for the combined 2nd-3rd vegetation classes predominantly describe values for the transit zone, calculated based on the Q_GRB dataset results are close to the obtained in previous studies: 0.971 and 1.054 for the 1st and combined 2nd-3rd vegetation classes respectively (for the 5th period). In comparison

with 2014 measurement campaign, results estimated for the second observation period are a little bit higher: 1.103 and 1.105 for the 1st and combined 2nd-3rd vegetation classes respectively (for the 6th period). These elevated values could be associated with the higher saturation with moisture of soils due to the delay at snow melting and the large amount of precipitation that fell by this time. On the other hand, the obtained α coefficient values for the Q_GTempCorr database for the same periods are in a state of disagreement with the results of previous studies: 1.181 and 0.7295 for the 1st vegetation class and 0.6844 and 0.9294 for the combined 2nd-3rd vegetation classes during the 2014 and 2015 measurement campaigns respectively. The main reason can be associated with an underestimation Q_GTempCorr values in comparison with Q_GRB.

5.2.2. Changing of surface resistance values during the measurement campaigns

In comparison with the PT approach, three meteorological variables have a significant impact on the ET estimations by PM method in addition to the available energy R_n-Q_G: r_a, VPD, and r_s. Surface resistance (r_s) characterizes the resistance of water that evaporates through the surface of plants. In case that the vegetation canopy doesn`t totally cover the soil surface, the value of r_s will be included the resistance of soil surface to ET process. According to the FAO [1998], the surface resistance could be described as the ratio between stomatal resistance of leaf - r_l (sm^{-1}) and LAI_{active} -active leaf area index (leaf area m^2 per ground area m^{-2}).

The LAI_{active} describes the leaf surface that actively participates in turbulent energy exchange processes. Mainly, LAI_{active} refers to the upper part of leaf. The LAI_{active} values vary greatly for various plant species. Nevertheless, for all vegetation types dynamic changes of LAI_{active} index is close to a bell shape, reaching the maximum at the period of flowering (FAO, 1998). The r_l describes the resistance stomatas to the transpiration via the leaf. As at the case with the LAI_{active} index, value of r_l varies for different vegetation types. Despite on this, a dynamic change of r_l value during the season also looks like a bell with the peak at the period of maximum growing (O`Tolle and Cruz, 1980). However, most of information about $r_l$ values links with the special investigations, which main aims are to estimate fluctuation of $r_l$ values under influence of different factors (O`Tolle and Cruz, 1980).

Dynamic changes of r_s values for the combination of combined 2nd-3rd vegetation classes estimated on the two datasets of ground heat flux estimates looks

close to bell-shape during the measurement campaigns (Figure 17). Corresponding changes of r_s values over the observation periods could be associated with the seasonal changes of the vegetation cover. Thus, at the beginning and the end of observation periods, r_s values for the combined 2^{nd}-3^{rd} vegetation classes are low. This could be linked that during these periods the plants have not been developed yet or have already withered. Moreover, at the start of observation periods the soil resistance to the evaporation processes was low due to an oversaturation with water. Nevertheless, plants have passed all stages of life over the measurement campaign. Based on the obtained results, we could say that the up to the period of maximum plants grow, the stomatal resistance of plants prevailed over the rate of leaves growing, which affected the gradual increase of r_s values. However, after plants reach their peak of growth, the situation changed to the opposite. Nevertheless, the dynamic change of r_s could be affected by different micrometeorological parameters (Figure11). Thus, the increase of r_s values for the combined 2^{nd}-3^{rd} vegetation classes during the first half of September 2015 (9 period) could be associated with the increased values of VPD (over 1 kPa).

However the influence of other meteorological variables on the estimation of r_s values could be clearly seen at the example of obtained results for 1^{st} vegetation class during 2014 and 2015 measurement campaign. Thus, changes of wind speed and as consequence r_a have serious effect on the obtained r_s values for 1^{st} vegetation class (Figure 11). Due to this fact, that r_a dynamic over the first measurement campaign was represented as a sequence shift of high and low values, the estimated results of r_s were close to the wave-form. However, an example of explicit influence of r_a on the r_s could be found during the second measurement campaign. Thus, gradual increases of r_a from low values to extremely high at the begging and middle of 2015 observation period with a small break at the second half of July lead to a close step-like dynamic pattern of r_s for the 1^{st} vegetation class over the measurement campaign. Such a close relationship could be associated with two factors. Firstly, due to the fact that 1^{st} vegetation class describes elevated areas, the changes in wind speed will be more significant in these areas. This has a serious impact on the r_s values via changes at r_l. Secondly, in this study r_s values were used as a fitting parameter, that were affected by side of different meteorological variables. Based on this assumption, even minor uncertainties of such meteorological variables as VPD and r_a could have a serious influence on the underestimation of r_s values.

According to the previous studies, at the river terrace part of Samoylov Island there dominate hygrophilous types of vegetation, r_s was calculated close to the 45 sm^{-1} (Kutzbach, 2006). Moreover, these results are close to obtained at the marshes of Alaska there r_s was amounted to 46±40 sm^{-1} (Liljedahl et al., 2011). Nevertheless, r_s values obtained at the low shrubs differ from the mentioned above: 175 sm^{-1} at five Alaska's site (Beringer et al., 2005) and 160 ± 70 sm^{-1} for arctic territories of Sweden (Kellner, 2001). Thus, calculated results based on the Q_GRB dataset for the maximum peak of plants development during the 2015 measurement campaign are close to the obtained in previous studies: 55.36 sm^{-1} and 85.06 sm^{-1} for the 1st and combined 2nd-3rd vegetation classes, respectively (6th period). In comparison with 2015 measurement campaign, results estimated for the first observation period are a little bit higher: 98.91 sm^{-1} and 98.11 sm^{-1} for the 1st and combined 2nd-3rd vegetation classes, respectively (5th period). These elevated values could be associated with the bigger impact during this period from the side of VPD and r_a fluctuations. On the other hand, obtained r_s values for the Q_GTempCorr database for the first measurement campaign are close to the results of previous studies: 57.57 sm^{-1} and 191 sm^{-1} for the 1st vegetation class and combined 2nd-3rd vegetation classes. Nevertheless, during the 2015 measurement campaign these dataset didn't allow to obtain well-fitted results: 183.6 sm^{-1} and 79.44 sm^{-1} for the 1st vegetation class and combined 2nd-3rd vegetation classes respectively. The main reason of such variability during the second season can be associated with an underestimation Q_GTempCorr values in comparison with Q_GRB and high effect from the r_a and VPD fluctuations over the observations.

5.2.3. Comparison of modeled evapotranspiration values by different approaches

Based on the comparison of correlation coefficient, it could be concluded that PT approach allows getting stronger correlation between the modeled and observed values of ET than PM method during both measurement campaigns. Thus, correlation value between the recorded and modeled values, based on the PT approach and Q_GRB database are 0.92 and 0.932, while PT method allows getting 0.899 and 0.891 for 2014 and 2015 measurement campaigns, respectively (Appendix, table 1-9). The Q_GTempCorr datasets also allow estimating quite high values of coefficient of correlation between modeled and recorded ET values: 0.834 and 0.835 for PT method and 0.86 and 0.821 for PM approach over the first and second measurement campaign respectively. However, calculations based on the Q_GTempCorr datasets are

characterized with lower correlation values than estimations based on Q_GRB. In the first case, presumably, Q_GTempCorr values were underestimated despite all adopted correction processes.

Nonetheless, PT does not allow receiving the best results of modeling over the whole observation seasons. Thus, according to the obtained coefficient of determination (R^2_{adj}) for each allotted period, PT approach allows to estimate better modeled results for the first half of measurement campaigns, while the PM – for the second (Appendix, table 1-9). This could be associated with several factors. Thus, from the beginning up to the middle of measurement campaigns, soils are oversaturated, which satisfies the conditions of application of PT method. Moreover, during these periods, vegetation is at the phenology stages of active growth that leads to that transpiration of moisture from soil prevails above evaporation via leaves. Nevertheless, than the mean daily ET rates decrease less than 0.15 mm, accounting into PM calculations influence of VPD, and r_a over the periods allows to get values estimated with higher accuracy than PT approach (Figure 11). Moreover, according to Kutzbach [2006], variations of r_s and VPD are strongly correlated to each other during the periods of maximum vegetation growth. Based on this close relationship and taking into account the VPD changes, PM approach allows obtaining better modeling results for short-term 4 period and 6 period during the first and second observation campaigns respectively.

5.3. Influence of hydrometeorological conditions on the evapotranspiration calculation

The large differences could be found between averages and mean daily rates of ET fluxes between the two measurement campaigns. According to Eaton and Rouse [2001], the high rates of ET at conditions of Canadian high latitude wetlands were well correlated with the high amount of precipitation. Based on this assumption, higher values of ET should be observed during the second measurement campaign, however, it is not so. Despite of this, results of this study indicate that during the relative dryer 2014 campaign, the mean value of ET is higher by 20% in comparison with the more humid second observation campaign (Figure 11). Similar results have already been obtained in previous studies (Wu et al., 2010, Liljedahl et al., 2011). This difference could be linked with lower R_n and predominance of cloudy conditions over the second observation campaign that effect on the decreased rates of ET in comparison with the first measurement campaign. Moreover, according to Wu [2010] and Liljedah [2011],

precisely the R_n, as well as closely related meteorological parameters, such as VPD, are the key factors that determine ET fluxes.

5.4. Analysis of spatial heterogeneity and upscale of modeled results

Based on the obtained data, the average value of fraction of the 1st vegetation class at the footprint area is reached only 33% during both campaigns (Figure 19). Nevertheless, during the periods when the footprint area was consisted of both significant fractions of 1st and combined 2nd-3rd vegetation classes, the greatest values of ET fluxes were recorded. Usually, during these periods, the winds from northwest, northeast and southeast directions were prevailed (Figure 20).

Moreover, at the directions with the maximal modeled values, could be observed the territorial proximity of the 1st and 3rd vegetation classes. In contrast, when the lowest values were recorded, wind prevailed mainly from the 1st or the 2nd vegetation class. Based on this, although the fraction of the 3rd vegetative class in the footprint area was small, the ET rates from these oversaturated soils with water are large, which have a significant effect on the recorded and modeled values (Figure 5).

As in the case of Q_G, obtained ET values could be compared with values observed at the river terrace. According to the Muster [2012], at the polygonal tundra environment, on the river terrace part of Samoylov Island during the July 21 – August 21, the mean daily ET values are 1.8±1.0 mm/day for wet and 1.0±0.7 mm/day for dry tundra. Compared to the results of the previous investigation on the Holocene river terrace, the mean daily ET values obtained at the modern floodplain are significantly lower. Thus, for the second measurement campaign, when the daily ET rates for the relatively dry and wet tundra environmental conditions are 0.4±0.21 mm/day and 0.75±0.3 mm/day respectively, the difference could be up to 2.5 times. In comparison with the first measurement campaign, the obtained ET rates are closer but still lower to values, which were estimated during the previous study: 0.6±0.26 mm/day and 1.05±0.42 mm/day for the 1st and combined 2nd and 3rd vegetation classes respectively. First of all, such differences can be associated with differences at environmental conditions of observation and differences at weather conditions during the observation periods.

According to the modeled results over the both measurement campaigns could be identified several differences between ET rates for 1 m^2 of the 1st and combined 2nd

and 3rd vegetation classes. Thus, ET values of combined 2nd and 3rd vegetation classes are in several times higher than ET rates of the 1st vegetation class. It could be linked with the higher amount of available moisture for the ET due that fact that water accumulates at the lowlands territories.

Moreover, the total ET rates over the two measurement campaigns for the 1st vegetation class are close to each other in comparison to the combined 2nd and 3rd vegetation classes. This can be associated with several factors. Firstly, due to the more developed root and canopy system, the ET rate from the 1st vegetation class is more stable (Liljedahl et al., 2011). Nevertheless, weather conditions also have effect on the ET rates and fluctuations over the season. Mainly due to that, the obtained ET values for the second observation campaign are lower than for the first. Moreover, based on the obtained data of ET rates, could be noted that the vegetation of lowlands and transitional areas are more vulnerable to the meteorological conditions in comparison with the vegetation of elevated territories. Secondly, the fluctuations of ET rates of the combined 2nd and 3rd vegetation classes are influenced by the groundwater level, which varies as a result of melting of permafrost and precipitation. As the 1st vegetation class describes elevated areas, such changes will not significantly affect the rate of ET from these territories.

Furthermore, obtained ET rates from 1 m^2 for each vegetation class allow upscaling modeled results to the whole floodplain territory. Thus, if the assumption that precipitation fell evenly throughout the floodplain territory will be accepted, the total amount of water that came at the form of rain during the June 18 – August 31 for the first measurement campaign is 72344.52 m, while for the second – 114327.38 m. According to the estimations over mentioned period, the ET rates for the territories of 1st vegetation class and combined 2nd and 3rd are: 10440.84 m and 72024.85 m for the first measurement campaign, while for the second 8856.45 m and 52943.31 m respectively. Thereby, based on the comparison of calculated total values for the whole floodplain area, during the 2014 measurement campaign ET rates were in 1.36 times higher than precipitation. These results well fit with the previous findings that the ET flux exceeds summer precipitation in summer and it is a major mechanism of summer water loss for Arctic areas (Rovanesk et al., 1996). In contrast to this, during the 2015 measurement campaign ET rates were in 0.54 times lower than precipitation. This could be explained by lower ET rates from the 1st and combined 2nd and 3rd vegetation classes due to a lower amount of available energy during the second measurement campaign.

Based on this, during the first measurement campaign at the soil could be formed oxic conditions, while for the second – anoxic. Thus, presumably, releasing of carbon from the soil occurs in two different forms: CO_2 and CH_4 respectively. Nevertheless, in order to ascertain of which conditions are established at the soils, when the ET prevails the precipitation and in opposite cases, further investigations of others elements of the hydrological cycle are needed.

6. Conclusion

This study has compared modeled ET values calculated using the Priestly-Taylor (PT) and Penman- Monteith (PM) approaches based on two different methods of ground heat flux estimations at a heterogeneous tundra landscape with variable mesorelief and vegetation cover by the example of an active floodplain on Samoylov Island in the Lena River Delta. The original ET data from the floodplain territories were calculated using the eddy covariance measurement technique.

Based on the comparison of correlation coefficient, PT approach allows getting stronger correlation between the modeled and observed values of ET than PM method for both measurement campaigns. Thus, correlation value between the recorded and modeled values, based on the PT approach and Q_GRB database are 0.92 and 0.932, while PT method allows getting 0.899 and 0.891 for 2014 and 2015 measurement campaigns, respectively. However, calculations based on the Q_GTempCorr datasets are characterized with lower correlation values than estimations based on Q_GRB. In the first case Q_GTempCorr values, presumably, were underestimated despite all adopted correction processes. Nonetheless, PT does not allow receiving the best results of modeling over the whole observation seasons. Thus, according to the obtained coefficient of determination (R^2_{adj}), PT approach allows estimating better modeled results for the first half of measurement campaigns, while the PM – for the second.

The large differences were found between averages and mean daily rates of ET fluxes between two measurement campaigns. Thus, the mean value of ET flux for 2014 measurement campaign is 0.057 ± 0.039 mm h^{-1}, while for 2015 it is 0.048 ± 0.035 mm h^{-1}. Results of this study indicate that during the relative dryer 2014 campaign, the mean value of ET is higher by 20% in comparison with the more humid second observation campaign. This difference is linked with lower R_n and predominance of cloudy conditions over the second observation campaign.

Based on the obtained data, the average value of fraction of the shrubs at the footprint area reached only 33% during both campaigns. Nevertheless, during the periods when the footprint area was consisted of both significant fractions of shrubs and sedges, the greatest values of ET fluxes were recorded. Usually, during these periods, the winds from northwest, northeast and southeast directions were prevailed. Thus, at the directions with the maximal modeled values, were observed the territorial proximity of the elevated and lowlands territories.

Furthermore, based on the comparison of calculated total values for the whole floodplain area, during the 2014 measurement campaign ET rates were in 1.36 times higher than precipitation, while for the 2015 in 0.54 times lower. Based on this, during the first measurement campaign at the soil could be formed oxic conditions, while for the second – anoxic. Thus, presumably, releasing of carbon from the soil occurs in two different forms: CO_2 and CH_4 respectively.

7. Acknowledgments

Firstly, I would like to thank Prof. Dr. Lars Kutzbach and Prof. Dr. Kirill Chistyakov for supervising this work and opportunity to expand my knowledge in the subject area. Secondly, thanks go to Norman Rößger for allowing me to use his eddy covariance data. I am grateful for the time and effort that you have taken to share your knowledge about Eddy covariance method, collected data, and programming in Matlab. I would like to acknowledge the help and advice of Prof. Dr. Igor Rusin, who explained his method of ground heat flux calculations and allowed to apply it in this study. I would also like to thank the M.Sc. Program for Polar and Marine Science (POMOR) for the opportunity to study interesting subjects and acquire my knowledge about the Arctic in all spheres of science. Special thanks go to my family and my friends for the great support and cheering me up when I needed it.

8. References

Almusaed, A., 2011. Evapotranspiration and Environmental Benefits. In Biophilic and Bioclimatic Architecture, Springer London. pp. 167-171.

Arft, A.M., Walker, M.D., Gurevitch, J.E.A., Alatalo, J.M., Bret-Harte, M.S., Dale, M., Diemer, M., Gugerli, F., Henry, G.H.R., Jones, M.H. and Hollister, R.D., 1999. Responses of tundra plants to experimental warming: Meta-analysis of the international tundra experiment. Ecological monographs, 69(4), pp.491-511.

Aubinet, M., Berbigier, P., Bernhofer, C.H., Cescatti, A., Feigenwinter, C., Granier, A., Grünwald, T.H., Havrankova, K., Heinesch, B., Longdoz, B. and Marcolla, B., 2005. Comparing CO 2 storage and advection conditions at night at different carboeuroflux sites. Boundary-Layer Meteorology, 116(1), pp.63-93.

Aubinet, M., Heinesch, B. and Longdoz, B., 2002. Estimation of the carbon sequestration by a heterogeneous forest: Night flux corrections, heterogeneity of the site and inter-annual variability. Global Change Biology, 8(11), pp.1053-1071.

Bai, J., Jia, L., Liu, S., Xu, Z., Hu, G., Zhu, M. and Song, L., 2015. Characterizing the footprint of eddy covariance system and large aperture scintillometer measurements to validate satellite-based surface fluxes. IEEE Geoscience and Remote Sensing Letters, 12(5), pp.943-947.

Baldocchi, D. 2005. http://nature.berkeley.edu/biometlab/espm129/pdf/Lecture 26 espm 129.pdf

Beer, C., 2008. Soil science: The Arctic carbon count. Nature Geoscience, 1(9): pp. 569-570.

Beltaos, S., 2002. Effects of climate on mid-winter ice jams. Hydrological Processes, 16(4), pp.789-804.

Billings, W.D. and Mooney, H.A., 1968. The ecology of arctic and alpine plants. Biological reviews, 43(4), pp.481-529.

Billings, W.D., Luken, J.O., Mortensen, D.A. and Peterson, K.M., 1982. Arctic tundra: A source or sink for atmospheric carbon dioxide in a changing environment?. Oecologia, 53(1), pp.7-11.

Blaney, H.F. and Criddle, W.D., 1962. Determining consumptive use and irrigation water requirements (No. 1275). US Department of Agriculture.

Boike, J., Grüber, M., Langer, M., Piel, K. and Scheritz, M., 2012. Orthomosaic Samoylov Island, Lena Delta, Siberia.

Boike, J., Kattenstroth, B., Abramova, E., Bornemann, N., Chetverova, A., Fedorova, I., Fröb, K., Grigoriev, M., Grüber, M., Kutzbach, L. and Langer, M., 2013. Baseline characteristics of climate, permafrost and land cover from a new permafrost observatory in the Lena River Delta, Siberia (1998-2011). Biogeosciences (BG), 10(3), pp.2105-2128.

Brown, J. and Haggerty, C., 1998. Permafrost digital databases now available. Eos, Transactions American Geophysical Union, 79(52), pp.634-634.

Brown, J., Hinkel, K.M. and Nelson, F.E., 2000. The circumpolar active layer monitoring (calm) program: Research designs and initial results 1. Polar geography, 24(3), pp.166-258.

Burba, G. and Anderson, D., 2007. Introduction to the eddy covariance method: General guidelines and conventional workflow. Li-Cor Biosciences, 141.

Burba, G.G., 2001. Illustration of flux footprint estimates affected by measurement height, surface roughness, and thermal stability. Automated Weather Stations for Applications in Agriculture and Water Resources management: Current Use and Future Perspectives. World Meteorological Organization, Lincoln, NE.

Burba, G.G., Anderson, D.J., Xu, L. and McDermitt, D.K., 2006, December. Additional term in the Webb-Pearman-Leuning correction due to surface heating from an open-path gas analyzer. In AGU Fall Meeting Abstracts.

Carey, S.K. and Woo, M.K., 1998. Snowmelt hydrology of two subarctic slopes, southern Yukon, Canada. Hydrology Research, 29(4-5), pp.331-346.

Clothier, B.E., Clawson, K.L., Pinter, P.J., Moran, M.S., Reginato, R.J. and Jackson, R.D., 1986. Estimation of soil heat flux from net radiation during the growth of alfalfa. Agricultural and forest meteorology, 37(4), pp.319-329.

Cohen, L.R., Raz-Yaseef, N., Curtis, J.B., Young, J.M., Rahn, T.A., Wilson, C.J., Wullschleger, S.D. and Newman, B.D., 2015. Measuring diurnal cycles of

evapotranspiration in the Arctic with an automated chamber system. Ecohydrology, 8(4), pp.652-659.

Connon, R.F., Quinton, W.L., Craig, J.R. and Hayashi, M., 2014. Changing hydrologic connectivity due to permafrost thaw in the lower Liard River valley, NWT, Canada. Hydrological Processes, 28(14), pp.4163-4178.

Davidson, E.A. and Janssens, I.A., 2006. Temperature sensitivity of soil carbon decomposition and feedbacks to climate change. Nature 440, 165e173.

De Bruin, H.A.R. and Holtslag, A.A.M., 1982. A simple parameterization of the surface fluxes of sensible and latent heat during daytime compared with the Penman-Monteith concept. Journal of Applied Meteorology, 21(11), pp.1610-1621.

Donchenko, R.V., 1987. Ice regime of rivers of the USSR. Gidrometeoizdat. (In Russian)

Eaton, A.K., Rouse, W.R., Lafleur, P.M., Marsh, P. and Blanken, P.D., 2001. Surface energy balance of the western and central Canadian subarctic: Variations in the energy balance among five major terrain types. Journal of Climate, 14(17), pp.3692-3703.

Eichinger, W.E., Parlange, M.B. and Stricker, H., 1996. On the concept of equilibrium evaporation and the value of the priestley-taylor coefficient. Water Resources Research, 32(1), pp.161-164.

Engstrom, R.N., Hope, A.S., Stow, D.A., Vourlitis, G.L. and Oechel, W.C., 2002. Priestley-Taylor alpha coefficient: variability and relationship to NDVI in arctic tundra landscapes. JAWRA Journal of the American Water Resources Association, 38(6), pp.1647-1659.

Eugster, W., Rouse, W.R., Pielke Sr, R.A., Mcfadden, J.P., Baldocchi, D.D., Kittel, T.G., Chapin, F.S., Liston, G.E., Vidale, P.L., Vaganov, E. and Chambers, S., 2000. Land–atmosphere energy exchange in Arctic tundra and boreal forest: available data and feedbacks to climate. Global change biology, 6(S1), pp.84-115.

Farouki, O.T., 1986. Thermal properties of soils.

Fedorova, I., Chetverova, A., Bolshiyanov, D., Makarov, A., Boike, J., Heim, B., Morgenstern, A., Overduin, P.P., Wegner, C., Kashina, V. and Eulenburg, A., 2015.

Lena Delta hydrology and geochemistry: long-term hydrological data and recent field observations. Biogeosciences, 12(2), pp.345-363.

Finnigan, J.J., 2004. A re-evaluation of long-term flux measurement techniques part II: coordinate systems. Boundary-Layer Meteorology, 113(1), pp.1-41.

Flint, A.L. and Childs, S.W., 1991. Use of the Priestley-Taylor evaporation equation for soil water limited conditions in a small forest clearcut. Agricultural and Forest Meteorology, 56(3-4), pp.247-260.

Foken, T. and Kretschmer, D., 1990. Stability dependence of the temperature structure parameter. Boundary-Layer Meteorology, 53(1), pp.185-189.

Foken, T. and Wichura, B., 1996. Tools for quality assessment of surface-based flux measurements. Agricultural and forest meteorology, 78(1), pp.83-105.

Foken, T., 1998. Die scheinbar ungeschlossene Energiebilanz am Erdboden-eine Herausforderung an die Experimentelle Meteorologie. Sitzungsberichte der Leibniz-Sozietät, 24(5), pp.131-150.

Foken, T., Göockede, M., Mauder, M., Mahrt, L., Amiro, B. and Munger, W., 2004. Post-field data quality control. In Handbook of micrometeorology (pp. 181-208). Springer Netherlands.

Foken, T., 2008. The energy balance closure problem: an overview. Ecological Applications, 18(6), pp.1351-1367.

Foken, T., 2017. Micrometeorology, 2nd edition. Berlin: Springer.

Food and Agriculture Organization of the United Nations (FAO), Doorenbos, J. and Kassam, A.H., 1977. FAO Irrigation and drainage paper. Food and Agriculture Organization of the United Nations.

Friborg, T., Soegaard, H., Christensen, T.R., Lloyd, C.R. and Panikov, N.S., 2003. Siberian wetlands: Where a sink is a source. Geophysical research letters, 30(21).

Fröb, K., 2011. Measuring and modeling of soil thermal properties and ground heat flux at two different sites at Lena Delta, Siberia (Doctoral dissertation, University of Leipzig).

Fuchs, M. and Hadas, A., 1972. The heat flux density in a non-homogeneous bare loessial soil. Boundary-layer meteorology, 3(2), pp.191-200.

Gao, Z., 2005. Determination of soil heat flux in a Tibetan short-grass prairie. Boundary-layer meteorology, 114(1), pp.165-178.

Gao, Z., Wang, L. and Horton, R., 2009. Comparison of six algorithms to determine the soil thermal diffusivity at a site in the Loess Plateau of China. Hydrology and Earth System Sciences Discussions, 6(2), pp.2247-2274.

Gash, J.H.C., 1986. A note on estimating the effect of a limited fetch on micrometeorological evaporation measurements. Boundary-Layer Meteorology, 35(4), pp.409-413.

Gedney, N., Cox, P.M. and Huntingford, C., 2004. Climate feedback from wetland methane emissions. Geophysical Research Letters, 31(20).

Giorgetta, M.A., Jungclaus, J., Reick, C.H., Legutke, S., Bader, J., Böttinger, M., Brovkin, V., Crueger, T., Esch, M., Fieg, K. and Glushak, K., 2013. Climate and carbon cycle changes from 1850 to 2100 in MPI-ESM simulations for the Coupled Model Intercomparison Project phase 5. Journal of Advances in Modeling Earth Systems, 5(3), pp.572-597.

Greco, S. and Baldocchi, D.D., 1996. Seasonal variations of CO2 and water vapour exchange rates over a temperate deciduous forest. Global Change Biology, 2(3), pp.183-197.

Grigoriev, M.N., 1993. Cryomorphogenesis of the Lena River mouth area. Siberian Branch, USSR Academy of Sciences, Yakutsk. (In Russian)

Harris, C., Arenson, L.U., Christiansen, H.H., Etzelmüller, B., Frauenfelder, R., Gruber, S., Haeberli, W., Hauck, C., Hoelzle, M., Humlum, O. and Isaksen, K., 2009. Permafrost and climate in Europe: Monitoring and modelling thermal, geomorphological and geotechnical responses. Earth-Science Reviews, 92(3), pp.117-171.

Hassan, R., Scholes, R. and Ash, N., 2005. Ecosystems and human wellbeing: volume 1: current state and trends.

Henry, G.H.R. and Molau, U., 1997. Tundra plants and climate change: the International Tundra Experiment (ITEX). Global Change Biology, 3(S1), pp.1-9.

Hobbie, J.E., 1980. Limnology of tundra ponds, Barrow, Alaska. Dowden, Hutchinson & Ross.

Hong, Y. and Gourley, J.J., 2014. Radar hydrology: principles, models, and applications. CRC Press.

Horst, T.W. and Lenschow, D.H., 2009. Attenuation of scalar fluxes measured with spatially-displaced sensors. Boundary-layer meteorology, 130(2), pp.275-300.

Hugelius, G., Strauss, J., Zubrzycki, S., Harden, J.W., Schuur, E., Ping, C.L., Schirrmeister, L., Grosse, G., Michaelson, G.J., Koven, C.D. and O'Donnell, J.A., 2014. Estimated stocks of circumpolar permafrost carbon with quantified uncertainty ranges and identified data gaps. Biogeosciences, 11(23), pp.6573-6593.

Ibrom, A., Dellwik, E., Flyvbjerg, H., Jensen, N.O. and Pilegaard, K., 2007. Strong low-pass filtering effects on water vapour flux measurements with closed-path eddy correlation systems. Agricultural and Forest Meteorology, 147(3), pp.140-156.

IPCC, 2001. climate change 2001: the scientific basis. Contribution of Working Group 1 to the Third Assessment Report of the Intergovernmental Panel on Climate Change, edited by JT Houghton, Y. Ding, DJ Griggs, M. Noguer, PJ van der Linden, X. Dai, K. Maskell and CA Johnson (eds). Cambridge University Press, Cambridge, UK, and New York, USA, 2001. ISBN 0-521-80767-0 (hardback). International Journal of Climatology, 22(9), pp. 1144-1144.

IPCC, 2007. Intergovernmental Panel on Climate Change, Climate Change 2007: The Physical Science Basis. Contribution of Working Group I to the Fourth Assessment Report of the Intergovernmental Panel on Climate Change. New York: Cambridge University Press, 996 pp.

Ivanov, V.V. and Piskun, A.A., 1999. Distribution of river water and suspended sediment loads in the deltas of rivers in the basins of the Laptev and East-Siberian Seas. In Land-Ocean Systems in the Siberian Arctic. Springer Berlin Heidelberg. pp. 239-250

Jorgenson, M.T., Racine, C.H., Walters, J.C. and Osterkamp, T.E., 2001. Permafrost degradation and ecological changes associated with a warming climate in central Alaska. Climatic change, 48(4), pp.551-579.

Jorgenson, M.T., Romanovsky, V., Harden, J., Shur, Y., O'Donnell, J., Schuur, E.A., Kanevskiy, M. and Marchenko, S., 2010. Resilience and vulnerability of permafrost to climate change This article is one of a selection of papers from The Dynamics of Change in Alaska's Boreal Forests: Resilience and Vulnerability in Response to Climate Warming. Canadian Journal of Forest Research, 40(7), pp.1219-1236.

Juszak, I., Erb, A.M., Maximov, T.C. and Schaepman-Strub, G., 2014. Arctic shrub effects on NDVI, summer albedo and soil shading. Remote sensing of environment, 153, pp.79-89.

Kane, D.L. and Chacho, E.F., 1990. Frozen ground effects on infiltration and runoff. In Cold Regions Hydrology and Hydraulics , ASCE. pp. 259-300.

Kane, D.L., Gieck, R.E. and Hinzman, L.D., 1990. Evapotranspiration from a small Alaskan arctic watershed. Hydrology Research, 21(4-5), pp.253-272.

Katul, G.G., Oren, R., Manzoni, S., Higgins, C. and Parlange, M.B., 2012. Evapotranspiration: a process driving mass transport and energy exchange in the soil-plant-atmosphere-climate system. Reviews of Geophysics, 50(3).

Koch, J.C., Kikuchi, C.P., Wickland, K.P. and Schuster, P., 2014. Runoff sources and flow paths in a partially burned, upland boreal catchment underlain by permafrost. Water Resources Research, 50(10), pp.8141-8158.

Koch, J.C., Runkel, R.L., Striegl, R. and McKnight, D.M., 2013. Hydrologic controls on the transport and cycling of carbon and nitrogen in a boreal catchment underlain by continuous permafrost. Journal of Geophysical Research: Biogeosciences, 118(2), pp.698-712.

Kormann, R. and Meixner, F.X., 2001. An analytical footprint model for non-neutral stratification. Boundary-Layer Meteorology, 99(2), pp.207-224.

Kutzbach, L., 2006. The exchange of energy, water and carbon dioxide between wet arctic tundra and the atmosphere at the Lena River Delta, Northern Siberia= Der Austausch von Energie, Wasser und Kohlendioxid zwischen arktischer Feuchtgebiets-

Trundra und der Atmosphäre im nordsibirischen Lena Delta. Berichte zur Polar-und Meeresforschung (Reports on Polar and Marine Research), p.541.

Landerer, F.W., Dickey, J.O. and Guentner, A., 2010. Terrestrial water budget of the Eurasian pan-Arctic from GRACE satellite measurements during 2003–2009. Journal of Geophysical Research: Atmospheres, D23. p.115

Leclerc, M.Y. and Foken, T., 2014. Footprints in micrometeorology and ecology. Heidelberg/New York/Dordrecht/London: Springer. p. 239

Leclerc, M.Y. and Thurtell, G.W., 1990. Footprint prediction of scalar fluxes using a Markovian analysis. Boundary-Layer Meteorology, 52(3), pp.247-258.

Lee, X., Liu, S., Xiao, W., Wang, W., Gao, Z., Cao, C., Hu, C., Hu, Z., Shen, S., Wang, Y. and Wen, X., 2014. The Taihu eddy flux network: an observational program on energy, water, and greenhouse gas fluxes of a large freshwater lake. Bulletin of the American Meteorological Society, 95(10), pp.1583-1594.

Liebethal, C. and Foken, T., 2007. Evaluation of six parameterization approaches for the ground heat flux. Theoretical and Applied Climatology, 88(1), pp.43-56.

Liljedahl, A.K., Hinzman, L.D., Harazono, Y., Zona, D., Tweedie, C.E., Hollister, R.D., Engstrom, R. and Oechel, W.C., 2011. Nonlinear controls on evapotranspiration in arctic coastal wetlands. Biogeosciences, 8(11), p.3375.

Makkink, G.F., 1957. Testing the Penman formula by means of lysimeters. J. Inst. of Water Eng., 11, pp.277-288.

Marín, E., 2011. Does Fourier's Law of Heat Conduction Contradict the Theory of Relativity?. Lat. Am. J. Phys. Educ. Vol, 5(2), p.402.

McGuire, A.D., Wirth, C., Apps, M., Beringer, J., Clein, J., Epstein, H., Kicklighter, D.W., Bhatti, J., Chapin III, F.S., De Groot, B. and Efremov, D., 2002. Environmental variation, vegetation distribution, carbon dynamics and water/energy exchange at high latitudes. Journal of Vegetation Science, 13(3), pp.301-314.

McMillen, R.T., 1988. An eddy correlation technique with extended applicability to non-simple terrain. Boundary-Layer Meteorology, 43(3), pp.231-245.

McNaughton, K.G. and Black, T.A., 1973. A study of evapotranspiration from a Douglas fir forest using the energy balance approach. Water Resources Research, 9(6), pp.1579-1590.

Mendez, J., Hinzman, L.D. and Kane, D.L., 1998. Evapotranspiration from a wetland complex on the Arctic coastal plain of Alaska. Hydrology Research, 29(4-5), pp.303-330.

Moncrieff, J., Clement, R., Finnigan, J. and Meyers, T., 2004. Averaging, detrending, and filtering of eddy covariance time series. In Handbook of micrometeorology, Springer Netherlands. pp. 7-31.

Monteith, J.L., 1965, July. Evaporation and environment. In Symp. Soc. Exp. Biol, Vol. 19, No. 205-23, p. 4.

Muster, S., Langer, M., Heim, B., Westermann, S. and Boike, J., 2012. Subpixel heterogeneity of ice-wedge polygonal tundra: a multi-scale analysis of land cover and evapotranspiration in the Lena River Delta, Siberia. Tellus B: Chemical and Physical Meteorology, 64(1), p.17301.

Myers-Smith, I.H., Forbes, B.C., Wilmking, M., Hallinger, M., Lantz, T., Blok, D., Tape, K.D., Macias-Fauria, M., Sass-Klaassen, U., Lévesque, E. and Boudreau, S., 2011. Shrub expansion in tundra ecosystems: dynamics, impacts and research priorities. Environmental Research Letters, 6(4), p.045509.

Oberbauer SF, Gillespie CT, Cheng W, Sala A, Gebauer R, Tenhunen JD, 1996.Diurnal and seasonal patterns of ecosystem CO_2 efflux from upland tundra in the foothills of the Brooks Range, Alaska, USA. Arctic and Alpine Research. 1996 Aug 1:328-38.

Oechel, W.C., Vourlitis, G.L., Hastings, S.J. and Zulueta, R.C., 2000. Acclimation of ecosystem CO_2 exchange in the Alaskan Arctic in response to decadal climate warming. Nature, 406(6799), p.978.

Osterkamp, T.E., 2005. The recent warming of permafrost in Alaska. Global and Planetary Change, 49(3), pp.187-202.

O'Toole, J.C. and Cruz, R.T., 1980. Response of leaf water potential, stomatal resistance, and leaf rolling to water stress. Plant physiology, 65(3), pp.428-432.

Pastick, N.J., Jorgenson, M.T., Wylie, B.K., Nield, S.J., Johnson, K.D. and Finley, A.O., 2015. Distribution of near-surface permafrost in Alaska: Estimates of present and future conditions. Remote Sensing of Environment, 168, pp.301-315.

Penman, H.L., 1948, April. Natural evaporation from open water, bare soil and grass. In Proceedings of the Royal Society of London A: Mathematical, Physical and Engineering Sciences The Royal Society, Vol. 193, No. 1032, pp. 120-145.

Peterson, K.M., Billings, W.D. and Reynolds, D.N., 1984. Influence of water table and atmospheric CO_2 concentration on the carbon balance of arctic tundra. Arctic and Alpine Research, pp.331-335.

Pidwirny, M., 2006. Periglacial processes and landforms. Fundamentals of Physical Geography, 2nd Edition.

Ping, C.L., Bockheim, J.G., Kimble, J.M., Michaelson, G.J. and Walker, D.A., 1998. Characteristics of cryogenic soils along a latitudinal transect in Arctic Alaska. Journal of Geophysical Research: Atmospheres, 103(D22), pp.28917-28928.

Polyakov, I.V., Bekryaev, R.V., Alekseev, G.V., Bhatt, U.S., Colony, R.L., Johnson, M.A., Maskshtas, A.P. and Walsh, D., 2003. Variability and trends of air temperature and pressure in the maritime Arctic, 1875–2000. Journal of Climate, 16(12), pp.2067-2077.

Priestley, C.H.B. and Taylor, R.J., 1972. On the assessment of surface heat flux and evaporation using large-scale parameters. Monthly weather review, 100(2), pp.81-92.

Priestley, C.H.B., 1959. Turbulent transfer in the lower atmosphere . Chicago: University of Chicago Press. pp. 543-561

Romanovsky, V.E., Smith, S.L. and Christiansen, H.H., 2010. Permafrost thermal state in the polar Northern Hemisphere during the international polar year 2007–2009: a synthesis. Permafrost and Periglacial processes, 21(2), pp.106-116.

Rößger N., Wille C., Kutzbach L., 2017, in preparation, Balancing and scaling methane fluxes ascertained in a heterogeneous tundra ecosystem of the Lena River Delta

Rouse, W.R., 2000. The energy and water balance of high-latitude wetlands: controls and extrapolation. Global Change Biology, 6(S1), pp.59-68.

Rouse, W.R., Carlson, D.W. and Weick, E.J., 1992. Impacts of summer warming on the energy and water balance of wetland tundra. Climatic Change, 22(4), pp.305-326.

Rovansek, R.J., Hinzman, L.D. and Kane, D.L., 1996. Hydrology of a tundra wetland complex on the Alaskan Arctic Coastal Plain, USA. Arctic and Alpine Research, pp.311-317.

Rusin, I.N. and Kukanova E.A., 2012. Evaluation of the ground heat flux in real-time based on the soil temperature data. Nauchnyj dialog, pp.302-315(7). (In Russian)

Rusin, I.N. Evaluation of the ground heat flux based on the soil temperature from different depth Trudy Glavnoj geofizicheskoj observatorii im. A.I. Voejkova, (570), pp.149-162. (In Russian)

Rutten, M.M., Steele-Dunne, S.C., Judge, J. and van de Giesen, N., 2010. Understanding heat transfer in the shallow subsurface using temperature observations. Vadose Zone Journal, 9(4), pp.1034-1045.

Saha, P., 2012. Modern climatology (Vol. 1). Allied Publishers.

Schuepp, P.H., Leclerc, M.Y., MacPherson, J.I. and Desjardins, R.L., 1990. Footprint prediction of scalar fluxes from analytical solutions of the diffusion equation. Boundary-Layer Meteorology, 50(1), pp.355-373.

Schuur, E.A., Crummer, K.G., Vogel, J.G. and Mack, M.C., 2007. Plant species composition and productivity following permafrost thaw and thermokarst in Alaskan tundra. Ecosystems, 10(2), pp.280-292.

Serreze, M.C. and Barry, R.G., 2011. Processes and impacts of Arctic amplification: A research synthesis. Global and Planetary Change, 77(1), pp.85-96.

Slatyer, R.O. and McIlroy, I.C., 1961. Practical Microclimatology. Practical Microclimatology.

Sonnentag, O., Van Der Kamp, G., Barr, A.G. and Chen, J.M., 2010. On the relationship between water table depth and water vapor and carbon dioxide fluxes in a minerotrophic fen. Global Change Biology, 16(6), pp.1762-1776.

Stannard, D.I., 1993. Comparison of Penman-Monteith, Shuttleworth-Wallace, and modified Priestley-Taylor evapotranspiration models for wildland vegetation in semiarid rangeland. Water Resources Research, 29(5), pp.1379-1392.

Stewart, R.B. and Rouse, W.R., 1976. A simple method for determining the evaporation from shallow lakes and ponds. Water Resources Research, 12(4), pp.623-628.

Strack, M., Waddington, J.M. and Tuittila, E.S., 2004. Effect of water table drawdown on northern peatland methane dynamics: Implications for climate change. Global Biogeochemical Cycles, 18(4).

Tennekes, H. and Lumley, J.L., 1972. A first course in turbulence. MIT press.

Tieszen, L.L., 1978. Vegetation and Production Ecology of an Alaskan Arctic Tundra, New York: Springer-Verlag, pp. 686

Trochim, E.D., Prakash, A., Kane, D.L. and Romanovsky, V.E., 2016. Remote sensing of water tracks. Earth and Space Science, 3(3), pp.106-122.

Tsejtin, G.H., 1953. On the question of the determination of certain thermal properties of the soil. Trudy GGO, (39), p.101.

Van Everdingen, R., 1998. revised May 2005. Multi-language glossary of permafrost and related ground-ice terms. Boulder, CO: National Snow and Ice Data Center/World Data Center for Glaciology.

Vickers, D. and Mahrt, L., 1997. Quality control and flux sampling problems for tower and aircraft data. Journal of Atmospheric and Oceanic Technology, 14(3), pp.512-526.

Vihma, T., Screen, J., Tjernström, M., Newton, B., Zhang, X., Popova, V., Deser, C., Holland, M. and Prowse, T., 2016. The atmospheric role in the Arctic water cycle: A review on processes, past and future changes, and their impacts. Journal of Geophysical Research: Biogeosciences, 121(3), pp.586-620.

Viswanadham, Y., Silva Filho, V.P. and Andre, R.G.B., 1991. The Priestley-Taylor parameter α for the Amazon forest. Forest Ecology and Management, 38(3-4), pp.211-225.

Walvoord, M.A., Voss, C.I. and Wellman, T.P., 2012. Influence of permafrost distribution on groundwater flow in the context of climate-driven permafrost thaw:

Example from Yukon Flats Basin, Alaska, United States. Water Resources Research, 48(7).

Wang, K. and Dickinson, R.E., 2012. A review of global terrestrial evapotranspiration: Observation, modeling, climatology, and climatic variability. Reviews of Geophysics, 50(2).

Webb, E.K., Pearman, G.I. and Leuning, R., 1980. Correction of flux measurements for density effects due to heat and water vapour transfer. Quarterly Journal of the Royal Meteorological Society, 106(447), pp.85-100.

Wille, C., Kutzbach, L., Sachs, T., Wagner, D. and Pfeiffer, E.V.A., 2008. Methane emission from Siberian arctic polygonal tundra: eddy covariance measurements and modeling. Global Change Biology, 14(6), pp.1395-1408.

Williams, C.A., Reichstein, M., Buchmann, N., Baldocchi, D., Beer, C., Schwalm, C., Wohlfahrt, G., Hasler, N., Bernhofer, C., Foken, T. and Papale, D., 2012. Climate and vegetation controls on the surface water balance: Synthesis of evapotranspiration measured across a global network of flux towers. Water Resources Research, 48(6).

Wilson, K., Goldstein, A., Falge, E., Aubinet, M., Baldocchi, D., Berbigier, P., Bernhofer, C., Ceulemans, R., Dolman, H., Field, C. and Grelle, A., 2002. Energy balance closure at FLUXNET sites. Agricultural and Forest Meteorology, 113(1), pp.223-243.

Woo, M.K., 1986. Permafrost hydrology in North America 1. Atmosphere-Ocean, 24(3), pp.201-234.

Woo, M.K., 2012. Permafrost hydrology. Springer Science & Business media.

Woo, M.K., Kane, D.L., Carey, S.K. and Yang, D., 2008. Progress in permafrost hydrology in the new millennium. Permafrost and Periglacial Processes, 19(2), pp.237-254.

Woo, M.K., Lewkowicz, A.G. and Rouse, W.R., 1992. Response of the Canadian permafrost environment to climatic change. Physical geography, 13(4), pp.287-317.

Wu, J., Kutzbach, L., Jager, D., Wille, C. and Wilmking, M., 2010. Evapotranspiration dynamics in a boreal peatland and its impact on the water and energy balance. Journal of Geophysical Research: Biogeosciences, 115(G4).

Yamazaki, Y., Kubota, J., Ohata, T., Vuglinsky, V. and Mizuyama, T., 2006. Seasonal changes in runoff characteristics on a permafrost watershed in the southern mountainous region of eastern Siberia. Hydrological Processes, 20(3), pp.453-467.

Zhang, T., 2005. Influence of the seasonal snow cover on the ground thermal regime: An overview. Reviews of Geophysics, 43(4).

Zhang, T., Heginbottom, J.A., Barry, R.G. and Brown, J., 2000. Further statistics on the distribution of permafrost and ground ice in the Northern Hemisphere 1. Polar Geography, 24(2), pp.126-131.

Zimov, S.A., Voropaev, Y.V., Semiletov, I.P., Davidov, S.P., Prosiannikov, S.F., Chapin, F.S., Chapin, M.C., Trumbore, S. and Tyler, S., 1997. North Siberian lakes: a methane source fueled by Pleistocene carbon. Science, 277(5327), pp.800-802.

Zubrzycki, S., Kutzbach, L., Grosse, G., Desyatkin, A. and Pfeiffer, E.M., 2012. Organic carbon and total nitrogen stocks in soils of the Lena River Delta. Biogeosciences Discussions, 9(12), p.17263.

9. Statement on the thesis originality

Herewith I, Vitalii Samoilenko, declare that I wrote the thesis independently and did not use any other resources than those named in the bibliography, and, in particular, did not use any internet resources except for those named in the bibliography. The master thesis has not been used previously as part of an examination. The master thesis has not been previously published.

Vitalii Samoilenko

Saint Petersburg, 25/08/2017

10. Appendix

Table 1. Estimated values of correction coefficient estimation between the Q_GRB and Q_GTemp datasets during the 2014 and 2015 measurement campaigns.

2014			2015		
Period	**Coefficient**	**Correlation**	**Period**	**Coefficient**	**Correlation**
18.06. -20.06.	2,649324	0,798958	09.06.-10.06.	6,174101	0,797807
20.06 – 24.06.	2,542622	0,899418	10.06.-11.06.	4,62695	0,603921
24.06.-26.06.	2,747837	0,657836	11.06.-12.06.	1,323605	0,280313
26.06.-28.06.	2,934856	0,828382	12.06.-12.06.	3,26649	0,875978
28.06.-30.06.	3,796532	0,871804	12.06.-13.06.	-0,16	0,069143
30.06.-01.07.	2,694562	0,506007	13.06.-13.06.	2,665165	0,725259
01.07.-03.07.	4,298411	0,782969	13.06.-15.06.	1,145263	0,43094
03.07.-05.07.	2,901577	0,769214	15.06.-15.06.	3,448494	0,844805
05.07.-06.07.	2,489723	0,90272	15.06.-16.06.	3,192745	0,885727
06.07.-08.07.	1,689518	0,498899	16.06.-17.06.	2,416725	0,731457
08.07.-10.07.	3,247488	0,849004	17.06.-18.06.	3,658072	0,824627
10.07.-11.07.	2,026462	0,802299	18.06.-20.06.	1,804722	0,685461
11.07.-13.07.	2,744812	0,681406	20.06.-21.06.	1,727701	0,689761
13.07.-14.07.	2,356406	0,679438	21.06.-23.06.	2,46697	0,75768
14.07.-17.07.	2,245381	0,834643	23.06.-24.06.	2,51909	0,892542
17.07.-21.07.	2,570708	0,859842	24.06.-25.06.	2,753743	0,889278
21.07.-23.07.	2,550633	0,808822	25.06.-27.06.	1,245619	0,496682
23.07.-27.07.	1,765375	0,613644	27.06.-27.06.	5,279403	0,959558
27.07.-29.07.	3,092148	0,787383	27.06.-29.06.	3,517373	0,891926
29.07.-01.08.	1,887796	0,815148	29.06.-02.07.	2,303966	0,770989
01.08.-04.08.	1,934751	0,795178	02.07.-06.07.	2,316938	0,747009
04.08.-07.08.	1,996266	0,822879	06.07.-07.07.	1,238359	0,687488
07.08.-10.08.	2,264465	0,843796	07.07.-09.07.	2,319931	0,860174

10.08.-12.08.	1,45751	0,569314	09.07.-12.07.	1,862911	0,769897
12.08.-14.08.	1,392753	0,702043	12.07.-15.07.	1,961387	0,815014
14.08.-17.08.	2,065373	0,852563	15.07.-16.07.	2,187817	0,73019
17.08.-20.08.	1,979541	0,888693	16.07.-21.07.	2,694131	0,754025
20.08.-23.08.	1,69821	0,839169	21.07.-23.07.	2,30442	0,652957
23.08.-26.08.	2,008185	0,907621	23.07.-27.07.	2,64951	0,779323
26.08.-29.08.	2,08679	0,885795	27.07.-31.07.	2,751021	0,80513
29.08.-31.08.	2,468103	0,89941	31.07.-02.08.	2,927201	0,855284
31.08.-03.09.	1,680773	0,701051	02.08.-04.08.	1,827047	0,675015
03.09.-05.09.	0,449275	0,194514	04.08.-07.08.	2,372166	0,804945
05.09.-08.09.	0,657517	0,255288	07.08.-11.08.	2,676495	0,824383
08.09.-10.09.	1,626044	0,884623	11.08.-14.08.	2,380381	0,818677
10.09.-13.09.	1,827655	0,84527	14.08.-16.08.	2,33085	0,721115
13.09.-15.09	1,599167	0,564977	16.08.-20.08.	1,857632	0,732606
			20.08.-23.08.	2,399845	0,7476
			23.08.-26.08.	2,829582	0,848819
			26.08.-29.08.	3,159954	0,879192
			29.08.-02.09.	2,182944	0,777183
			02.09.-03.09.	2,65902	0,885005
			03.09.-04.09.	2,234418	0,941867
			04.09.-07.09.	1,38547	0,780399
			07.09.-10.09.	1,962185	0,892934
			10.09.-12.09.	1,7704	0,816009
			12.09.-14.09.	1,759695	0,855113
			14.09.-17.09.	1,715367	0,802888
			17.09.-20.09.	1,778262	0,693203
			20.09.-23.09.	1,556876	0,482014

Table 2. Outcome of the estimation for α coefficient based on the solution of PT approach for each *i* vegetation class based on the Q_GRB dataset using the Ordinary Least Squares method for 2014.

	1	**2**	**3**	**4**	**5**	**6**	**7**	**8**	**9**	**For the whole period**
Date	18.06. - 28.06.	28.06. - 14.07.	14.07. - 27.07.	27.07. - 01.08.	01.08. - 10.08.	10.08. - 14.08.	14.08. - 29.08.	29.08. - 08.09.	08.09. - 15.09.	18.06. - 15.09.
α_Veg1	0.7585 ± 0.1299	0.8264 ± 0.0756	1.077 ± 0.056	1.122± 0.079	0.9707 ± 0.1483	1.354 ± 0.156	0.8829 ± 0.0873	1.29 ± 0.177	0.3459 ± 0.207	
α_Veg2+3	1.246 ± 0.056	1.009 ± 0.037	0.93 ± 0.0641	0.8737 ± 0.0325	1.054± 0.067	1.545 ± 0.269	1.392 ± 0.102	1.662 ± 0.228	1.285 ± 0.195	
R^2_{adj}	0.7641	0.8179	0.8653	0.9288	0.821	0.6953	0.6951	0.2993	0.3197	0.92
RMSE	0.0242	0.0244	0.0157	0.016	0.0157	0.0324	0.026	0.0346	0.0228	
Ω1, % of total	25.81	26	41.96	17.37	19.66	40.5	43.1	43.5	43.01	33.85
Ω2, % of total	54.98	53.34	42.36	58.37	55.33	39.92	39.65	37.67	37.01	46.61
Ω3, % of total	8.4	7.91	6.08	7.65	8.81	4.35	4.96	4.89	4.41	6.52
Numbers of observations	328	569	369	161	264	132	507	292	227	2839

Table 3. Outcome of the estimation for α coefficient based on the solution of PM approach for each *i* vegetation class based on the Q_GRB dataset using the Ordinary Least Squares method for 2014.

	1	**2**	**3**	**4**	**5**	**6**	**7**	**8**	**9**	**For the whole period**
Date	18.06. - 28.06.	28.06. - 14.07.	14.07. - 27.07.	27.07. - 01.08.	01.08. - 10.08.	10.08. - 14.08.	14.08. - 29.08.	29.08. - 08.09.	08.09. - 15.09.	18.06. - 15.09.
α_Veg1, sm^{-1}	94.93 ± 29.87	193.6± 30.5	127.6± 14.5	185.4± 21.2	98.91 ± 35.09	119.9 ± 12.9	153.3 ± 17.7	75.84 ± 12.34	189.1± 57.1	
α_Veg2+3, sm^{-1}	39.44 ± 5.86	68.88 ± 4.72	97.39 ± 12.91	94.95 ± 5.04	98.11± 16.49	75.74 ± 15.25	43.92 ± 5.66	15.56 ± 5.37	63.8 ± 16.05	
R^2_{adj}	0.718	0.8051	0.8623	0.9516	0.7474	0.8847	0.7644	0.5293	0.6008	0.899
RMSE	0.0265	0.0252	0.0159	0.0132	0.0187	0.02	0.0299	0.0284	0.0175	
Ω1, % of total	25.81	26	41.96	17.37	19.66	40.5	43.1	43.5	43.01	33.85
Ω2, % of total	54.98	53.34	42.36	58.37	55.33	39.92	39.65	37.67	37.01	46.61
Ω3, % of total	8.4	7.91	6.08	7.65	8.81	4.35	4.96	4.89	4.41	6.52
Numbers of observations	328	569	369	161	264	132	507	292	227	2839

Table 4. Outcome of the estimation for α coefficient based on the solution of PT approach for each *i* vegetation class based on the Q_GTempCorr dataset using the Ordinary Least Squares method for 2014.

	1	**2**	**3**	**4**	**5**	**6**	**7**	**8**	**9**	**For the whole period**
Date	18.06. - 28.06.	28.06. - 14.07.	14.07. - 27.07.	27.07. - 01.08.	01.08. - 10.08.	10.08. - 14.08.	14.08. - 29.08.	29.08. - 08.09.	08.09. - 15.09.	18.06. - 15.09.
α_Veg1	0.5732 ± 0.1341	0.606 ± 0.0675	0.8689 ± 0.0672	0.9228± 0.1102	1.181± 0.182	1.158 ± 0.119	0.8799 ± 0.0874	1.249 ± 0.239	0.2065 ± 0.182	
α_Veg2+3	0.9443 ± 0.0597	0.782 ± 0.0334	0.637 ± 0.0735	0.6524 ± 0.041	0.6844± 0.0832	1.113 ± 0.178	1.169 ± 0.096	1.426 ± 0.291	1.105 ± 0.16	
R^2_{adj}	0.49	0.7125	0.6836	0.7942	0.5824	0.7158	0.5962	0.2216	0.3018	0.834
RMSE	0.0359	0.0302	0.0235	0.0267	0.0299	0.0313	0.0296	0.0454	0.0229	
Ω1, % of total	27.15	26.39	42.59	17.32	22.1	39.81	42.36	43.06	40.75	33.62
Ω2, % of total	54.17	53.39	41.94	59.88	53.97	40.5	10.34	37.97	38.57	46.86
Ω3, % of total	8.26	7.88	6.06	7.6	8.73	4.43	5.09	4.96	4.74	6.58
Numbers of observations	394	666	429	187	367	138	587	306	266	3331

Table 5 Outcome of the estimation for α coefficient based on the solution of PM approach for each *i* vegetation class based on the Q_GTempCorr dataset using the Ordinary Least Squares method for 2014.

	1	**2**	**3**	**4**	**5**	**6**	**7**	**8**	**9**	**For the whole period**
Date	18.06. - 28.06.	28.06. - 14.07.	14.07. - 27.07.	27.07. - 01.08.	01.08. - 10.08.	10.08. - 14.08.	14.08. - 29.08.	29.08. - 08.09.	08.09. - 15.09.	18.06. - 15.09.
α_Veg1, sm^{-1}	146 ± 50.4	216.4± 36.5	134.5± 15.8	204.6± 44.6	57.57 ± 23.41	118.8 ± 12.9	168.7 ± 24.4	72± 13.2	206± 65.6	
α_Veg2+3, sm^{-1}	58.19 ± 8.46	94.2 ± 6.6	170.4 ± 25	135.4 ± 12.4	191± 41.2	110.7 ± 21.4	49.96 ± 7.65	16.57 ± 6.41	86.42 ± 20.58	
R^2_{adj}	0.5279	0.7228	0.783	0.8164	0.5349	0.8568	0.6198	0.4042	0.5316	0.835
RMSE	0.0346	0.0296	0.0195	0.0252	0.0316	0.0222	0.0288	0.0317	0.0188	
Ω1, % of total	27.15	26.39	42.59	17.32	22.1	39.81	42.36	43.06	40.75	33.62
Ω2, % of total	54.17	53.39	41.94	59.88	53.97	40.5	10.34	37.97	38.57	46.86
Ω3, % of total	8.26	7.88	6.06	7.6	8.73	4.43	5.09	4.96	4.74	6.58
Numbers of observations	394	666	429	187	367	138	587	306	266	3331

Table 6. Outcome of the estimation for α coefficient based on the solution of PT approach for each *i* vegetation class based on the Q_GRB dataset using the Ordinary Least Squares method for 2015.

	1	**2**	**3**	**4**	**5**	**6**	**7**	**8**	**9**	**10**	**For the whole period**
Date	09.06. - 17.06.	17.06 - 27.06.	27.06. - 16.07.	27.07 - 31.07.	31.07. - 11.08.	11.08. - 20.08.	20.08. - 02.09.	02.09. - 04.09.	04.09. - 10.09.	10.09. - 23.09.	09.06. - 23.09.
α_Veg1	1.248 ± 0.077	0.7554 ± 0.1068	0.7718 ± 0.0916	1.125± 0.104	0.953 ± 0.081	1.103 ± 0.181	0.9575 ± 0.1305	0.9205 ± 0.3785	0.5112 ± 0.1018	0.7344 ± 0.1358	
α_Veg2+3	1.014 ± 0.04	1.469± 0.092	1.094 ± 0.065	1.014 ± 0.063	0.9541± 0.0469	1.105 ± 0.105	1.436 ± 0.129	0.8158 ± 0.3082	0.7779 ± 0.1719	0.7982 ± 0.1147	
R^2_{adj}	0.898	0.78	0.7502	0.7957	0.8552	0.6976	0.5802	0.668	0.655	0.3012	0.932
RMSE	0.017	0.0214	0.0246	0.0171	0.0161	0.019	0.0239	0.0154	0.0126	0.0126	
Ω1, % of total	31.67	43.56	37.24	38.13	21.33	31.39	37.88	37.29	46.21	38.05	35.79
Ω2, % of total	47.02	36.83	43.33	42.94	55.47	48.37	40.08	41.9	34.84	39.67	43.48
Ω3, % of total	9.59	7.83	7.37	7.49	9.6	6.66	6.05	6.99	5.38	6.29	7.41
Numbers of observations	293	279	626	346	364	252	346	108	179	421	3194

Table7. Outcome of the estimation for α coefficient based on the solution of PM approach for each *i* vegetation class based on the Q_GRB dataset using the Ordinary Least Squares method for 2015.

	1	**2**	**3**	**4**	**5**	**6**	**7**	**8**	**9**	**10**	**For the whole period**
Date	09.06. - 17.06.	17.06 - 27.06.	27.06. - 16.07.	27.07 - 31.07.	31.07. - 11.08.	11.08. - 20.08.	20.08. - 02.09.	02.09. - 04.09.	04.09. - 10.09.	10.09. - 23.09.	09.06. - 23.09.
α_Veg1, sm^{-1}	38.89± 9.35	146.2± 42.7	336.6± 85.9	16.09± 8.51	139.9 ± 24.1	55.36 ± 22.85	277 ± 69.6	485.7± 323.7	727.6± 177.3	374.9 ± 91.6	
α_Veg2+3, sm^{-1}	29.68 ± 4.53	7.01 ± 4.35	46.45 ± 5.94	90.9 ± 14.6	54.27± 5.5	85.06 ± 16.34	45.08 ± 9.34	37.31 ± 11.83	92.44 ± 19.96	79.25 ± 15.14	
R^2_{adj}	0.8191	0.7044	0.6805	0.724	0.8548	0.7243	0.4846	0.801	0.7958	0.4414	0.891
RMSE	0.0226	0.0248	0.0278	0.0198	0.0161	0.0181	0.0265	0.0119	0.0097	0.0112	
Ω1, % of total	31.67	43.56	37.24	38.13	21.33	31.39	37.88	37.29	46.21	38.05	35.79
Ω2, % of total	47.02	36.83	43.33	42.94	55.47	48.37	40.08	41.9	34.84	39.67	43.48
Ω3, % of total	9.59	7.83	7.37	7.49	9.6	6.66	6.05	6.99	5.38	6.29	7.41
Numbers of observations	293	279	626	346	364	252	346	108	179	421	3194

Table 8. Outcome of the estimation for α coefficient based on the solution of PT approach for each *i* vegetation class based on the Q_GTempCorr dataset the Ordinary Least Squares method for 2015.

	1	**2**	**3**	**4**	**5**	**6**	**7**	**8**	**9**	**10**	**For the whole period**
Date	09.06. - 17.06.	17.06 - 27.06.	27.06. - 16.07.	27.07 - 31.07.	31.07. - 11.08.	11.08. - 20.08.	20.08. - 02.09.	02.09. - 04.09.	04.09. - 10.09.	10.09. - 23.09.	09.06. - 23.09.
α_Veg1	0.8147 ± 0.0927	0.5437 ± 0.1057	0.7686 ± 0.0838	0.8755± 0.1011	0.8586 ± 0.0859	0.7295 ± 0.1253	0.8678 ± 0.1214	0.8147 ± 0.2913	0.467 ± 0.0865	0.5838 ± 0.101	
α_Veg2+3	0.7443 ± 0.0497	1.248 ± 0.101	0.8226 ± 0.061	0.8371 ± 0.0645	0.7801± 0.0502	0.9294 ± 0.0866	1.16 ± 0.117	0.8093 ± 0.2397	0.5556 ± 0.1426	0.6623± 0.091	
R^2_{adj}	0.6881	0.542	0.6108	0.655	0.753	0.6069	0.5189	0.7218	0.5038	0.2955	0.86
RMSE	0.0294	0.0305	0.0311	0.0219	0.0212	0.0214	0.0257	0.0136	0.0148	0.0126	
Ω1, % of total	32.59	44.98	38.47	38.51	21.99	33.63	39.53	38.13	48.18	38.92	37.16
Ω2, % of total	46.49	36.13	42.38	42.45	54.79	46.69	38.4	41.67	33.53	38.97	42.39
Ω3, % of total	9.27	7.36	6.96	7.32	9.5	6.41	5.63	6.94	5.15	6.17	7.1
Numbers of observations	333	331	762	379	395	278	413	117	218	503	3718

Table 9. Outcome of the estimation for α coefficient based on the solution of PM approach for each *i* vegetation class based on the Q_GTempCorr dataset the Ordinary Least Squares method for 2015.

	1	**2**	**3**	**4**	**5**	**6**	**7**	**8**	**9**	**10**	**For the whole period**
Date	09.06. - 17.06.	17.06 - 27.06.	27.06. - 16.07.	27.07 - 31.07.	31.07. - 11.08.	11.08. - 20.08.	20.08. - 02.09.	02.09. - 04.09.	04.09. - 10.09.	10.09. - 23.09.	09.06. - 23.09.
α_Veg1, sm^{-1}	159.4 ± 50.4	350.3± 136.3.5	403.7± 105.3	44.38± 15.39	174.4 ± 37.6	183.6 ± 51.4	284.4 ± 72.8	573.7± 374	561.4± 119.2	381.4 ± 81.3	
α_Veg2+3, sm^{-1}	43.94 ± 7.72	7.64 ± 4.69	58.45 ± 7.27	104.5 ± 18.8	70.03± 8.63	79.44 ± 13.1	59.94 ± 11.8	44.4 ± 13.02	180.3± 43.5	103.6± 17.6	
R^2_{adj}	0.5191	0.4971	0.5678	0.5675	0.7221	0.6206	0.4105	0.7602	0.6453	0.428	0.821
RMSE	0.0365	0.032	0.0328	0.0246	0.0225	0.021	0.0285	0.0126	0.0125	0.0114	
Ω1, % of total	32.59	44.98	38.47	38.51	21.99	33.63	39.53	38.13	48.18	38.92	37.16
Ω2, % of total	46.49	36.13	42.38	42.45	54.79	46.69	38.4	41.67	33.53	38.97	42.39
Ω3, % of total	9.27	7.36	6.96	7.32	9.5	6.41	5.63	6.94	5.15	6.17	7.1
Numbers of observations	333	331	762	379	395	278	413	117	218	503	3718